Critical advances in the field of magnetron sputtered bioactive glass thin-films: An analytical review

Applied Surface Science 646 (2024) 158760

Contents lists available at ScienceDirect

Applied Surface Science

journal homepage: www.elsevier.com/locate/apsusc

Critical advances in the field of magnetron sputtered bioactive glass thin-films: An analytical review

George E. Stan [a,*], Maziar Montazerian [b,c,*], Adam Shearer [c], Bryan W. Stuart [d], Francesco Baino [e,*], John C. Mauro [c], José M.F. Ferreira [f,g,*]

[a] National Institute of Materials Physics, 077125 Magurele, Romania
[b] Northeastern Laboratory for Evaluation and Development of Biomaterials, Federal University of Campina Grande, 58429-900 Campina Grande, PB, Brazil
[c] Department of Materials Science and Engineering, The Pennsylvania State University, 16802 University Park, PA, USA
[d] Advanced Materials Research Group, Faculty of Engineering, University of Nottingham, NG7 2RD, UK
[e] Institute of Materials Physics and Engineering, Department of Applied Science and Technology, Politecnico di Torino, 10129 Torino, Italy
[f] CICECO Aveiro Institute of Materials, Department of Materials and Ceramics Engineering, University of Aveiro, 3810-193 Aveiro, Portugal
[g] Łukasiewicz Research Network – Institute of Microelectronics and Photonics, 02–668 Warsaw, Poland

ARTICLE INFO

Keywords:
Bioceramics
Bioactive glass
Magnetron sputtering
Thin-films
Implants
Bone regeneration

ABSTRACT

Bioactive glasses (BGs) are known for their selective ability to (*i*) form a mechanically strong interfacial bond with hard (bone) or soft tissues (gingivae or cartilages) (*i.e.*, silica-, silica-phosphate-, phosphate-, borate-phosphate-, or silica-phosphate-borate-based BGs); or (*ii*) serve as reservoirs for fast-release of therapeutic (osteogenic, angiogenic, anticarcinogenic, or antimicrobial) ions (*i.e.*, phosphate-based BGs and mesoporous BGs). The strength of the bone bond yielded by the osteoproductive-capable BGs is generally equivalent to, or higher than the bone strength. The resorbability of phosphate-based BG is dependent on the content of network formers and cross-linkers. All BGs elicit excellent biochemical compatibility. However, their fracture toughness is typically less than and the elastic modulus is greater than those of bone, indicating that most BGs have sub-optimal biomechanical compatibility when used in load-bearing applications. One promising approach to overcome this problem is the development of BGs in coating form, applied to the surface of load-bearing endosseous implants. This work critically assesses BG thin-layers fabricated by the radio-frequency magnetron sputtering method, an industry-ready large-scale physical vapour deposition technology. It is demonstrated that, despite the relative lack of attention paid to this technology, it enables the development of unique BG coatings with efficacious therapeutic capabilities. Here, we present an overview of the most relevant developments achieved thus far, along with the remarkable advantages, drawbacks to overcome, and future perspectives with the intention of highlighting the vast possibilities of this specific field of research.

1. Introduction

Load-bearing endosseous implants are typically made from medical-grade metallic alloys, with the titanium-based ones currently dominating the global market. The implants industry is predicted to increase rapidly in response to rising health and societal demands. For example, according to the recent Grand View Research's report, the worldwide market for dental implants is projected to grow from its value of $4.6 billion in 2020 to $9.62 billion in 2030, fostering a compound annual growth rate (CAGR) of 9.8% [1]. Despite their proven biocompatibility and outstanding mechanical performance, metallic implants require long healing times because they lack bioactivity, osteointegration, and therapeutic functions. Hence, they cannot contribute to the bonding and healing processes. Currently, coating the metallic and polymeric implants with bioactive and functional materials is being attempted to overcome these drawbacks [2].

* Corresponding authors at: National Institute of Materials Physics, 077125 Magurele, Romania (G.E. Stan). Department of Materials Science and Engineering, The Pennsylvania State University, 16802 University Park, PA, USA (M. Montazerian). Institute of Materials Physics and Engineering, Department of Applied Science and Technology, Politecnico di Torino, 10129 Torino, Italy (F. Baino). CICECO Aveiro Institute of Materials, Department of Materials and Ceramics Engineering, University of Aveiro, 3810-193 Aveiro, Portugal (J.M.F. Ferreira).

E-mail addresses: george_stan@infim.ro (G.E. Stan), mbm6420@psu.edu (M. Montazerian), francesco.baino@polito.it (F. Baino), jmf@ua.pt, jose.ferreira@imif.lukasiewicz.gov.pl (J.M.F. Ferreira).

https://doi.org/10.1016/j.apsusc.2023.158760
Received 15 September 2023; Received in revised form 26 September 2023; Accepted 25 October 2023
Available online 28 October 2023

Bioactive glasses (BGs), possessing outstanding biological properties beyond hard tissue regeneration applications [3,4], are projected to produce a revolution in the field of long-lasting, fast-healing, bacterial infection-protected cementless joint endoprostheses and dental implants coatings [5–11]. Currently, commercially available implants are coated with thick layers (>50 μm) of hydroxyapatite (HA) using the plasma spraying processes [12]. This is the most widespread technique for HA deposition [13] and, also the only process approved by the Food and Drug Administration (FDA) to coat clinical-ready endosseous implants [14]. Thus, it made sense for the research community to first focus on applying the thermal spray approach toward BG coatings, including several technological variants: atmospheric plasma spraying [15,16], liquid precursor plasma spraying [17,18], suspension plasma spraying [19,20], flame spraying/high velocity suspension flame spraying [21,22], high velocity oxy fuel (SHVOF) thermal spray [23] or cold spraying [24]. Despite demonstrating suitable biological performance, proper adherence of thermally sprayed coatings to the substrate remains one of the main drawbacks limiting their progress [25]. Potential solutions such as pre-heating of the substrate, introduction of bonding layers, or reduction of the coefficient of thermal expansion of BG without compromising its biological performance are envisaged [25,26]. Alternatively, competing (*i*) thick coating (>5 μm) and (*ii*) thin-film (<5 μm) deposition methods were advanced, including: (*i*) enamelling/glazing [27–30] or electrophoretic deposition [31–33], and (*ii*) sol–gel [34,35], pulsed laser deposition (PLD) [36–39], pulsed electron deposition [40,41], ion-beam sputtering [42,43] or radio-frequency magnetron sputtering (RF-MS) [44–51]. While many topical studies claim of being oriented towards implant coatings, research endeavours truly tackling BG-coating of actual endosseous implant with 3D profiles (and not flat substrates) are still rare. A few 3D attempts have been made by plasma spraying [52], enamelling/glazing [29,53], sol–gel [34], and radio-frequency magnetron sputtering [54–56]. Although known as a well-established deposition technology and employed with great success for decades in the decorative and electronics industries, RF-MS has been rather rarely approached for the deposition of BG coatings, going either unnoticed [2,8,10,57,58], or being just briefly referred to as variant [6,7,9,59–61] in the numerous topical reviews published to date. However, the advances made in RF-MS deposition of BGs, which accelerated in the last decade, make an analytical recapitulation of their fast-forwarding progression toward real-life biomedical applications mandatory. In this pursue, here, a critical review and a snapshot of the future potential of BG thin-films fabricated by RF-MS are given.

2. Sputtering: A brief historical and working principle overview

Efforts devoted to the development of BG coatings (for 316L stainless-steel- and alumina-based implants) were done shortly after the invention of the 45S5-Bioglass® formulation [62] by the research group led by Larry L. Hench, the founder of bioactive glasses. Flame spray was first explored (in 1972) as a deposition technique [63,64], followed by immersion dipping (in 1976) [65,66]. Yet again, L.L. Hench performed the first studies (reported in 1982 [42]) on the deposition of BG by one of the sputtering variants existing at that time, *i.e.*, ion beam sputtering (IBS). Both 45S5-Bioglass® ($46.1SiO_2$–$26.9CaO$–$2.6P_2O_5$–$24.4Na_2O$ (mol%)) and 52S4.6 ($52.1SiO_2$–$23.8CaO$–$2.6P_2O_5$–$21.5Na_2O$ (mol%)) were used to prepare films by IBS with thicknesses between 0.5 and 4 μm on 316L stainless-steel, alumina, and poly(methyl methacrylate) (PMMA) substrates. Only the thicker sputtered films were able to achieve adequate substrate coverage. *In vivo* experiments on Sprague–Dawley rats showed that BG-coated PMMA substrates produced the most promising outcomes after implantation. Furthermore, it was discovered that collagen could adhere to the BG-coated surface, indicating tissue adhesion.

In spite of an excellent control over deposition variables, translated into the possibility to engineer the stoichiometry of the deposits with higher accuracy, IBS has not yet been able to achieve reliable large-substrate coverage, making it less attractive for industrial application [67]. A further attempt at IBS deposition was recorded in 2002, when Wang *et al.* [43] employed a low silica BG formulation (SiO_2–35, CaO–50, P_2O_5–15 (mol%)) to deposit dense, highly adherent films capable of inducing good osteoblast cell proliferation.

The sputtering phenomenon was first reported by Sir W.R. Grove 1852 (while investigating discharge tubes with silver needle cathode), whilst F.M. Penning is credited with the conception of magnetron sputtering in 1936, and the proposal of the cylindrical magnetron ("Penning cell") concept [68]. Significant strides begun after the independent introduction of the planar magnetron sources by A.M. Dorodnov (in 1973) [69] and J.S. Chapin (in 1974) [70]. The employment of high-voltage alternating current at radio-frequency (in the range of 0.5–30 MHz, most often of 1.78, 5.28, 13.56, and 27.12 MHz) [67,71], instead of the direct current, enabled the sputtering of virtually any material, including dielectrics [72], revolutionizing the field and paving the way toward commercially available radiofrequency (RF)-magnetron sputtering (MS) systems in the early 1980s. With time, RF-MS emerged as one of the mainstream industrial processes for fabricating coatings from a plethora of materials [67,73]. RF-MS yields a series of notable advantages such as: (*i*) flexibility and reproducibility in sputtering all inorganic materials; (*ii*) reasonable deposition rates for dielectrics (if sub-micron thick layers are intended, as is the case in the semiconductor industry); (*iii*) excellent purity of films; (*iv*) remarkable high adherence of films to substrates; (*v*) ability to easily manipulate film properties by changing process variables (*i.e.*, electric power density, working gas pressure, working gas composition, target-to-substrate distance, substrate polarisation or substrate temperature); (*vi*) low temperature operation; (*vii*) facile automation; and, importantly (*viii*) exceptional uniformity (in terms of both thickness and stoichiometry) over large-area substrates [67,73,74]. Some studies highlight the main drawback of RF-MS as being the "line-of-sight" specificity of the process, which would make the coating of fixtures with complicated geometries virtually impossible. The simple translation/rotation of the 3D substrate is however a facile and efficient solution to overcome such a deficit [55]. There were, however, limitations in achieving coverage of samples with high aspect ratio features which has been in-part improved by ionised physical vapour deposition (PVD) techniques such as high-power impulse magnetron sputtering (HiPIMS).

Fig. 1 depicts a schematic illustration of the magnetron sputtering setup, which in the simplest concept consists of: a high-vacuum chamber (incorporating the magnetron cathode/guns, substrate holders, various biasing and heating facilities, *in situ* measurement/analysis systems); vacuum system; electrical (DC, RF, pulsed DC or HiPIMS) generators; gas sources with flowmeters and controllers; and water-cooling systems for guns and pumps. To ensure the high purity of the films, the chamber is first evacuated down by high-vacuum pump systems to a base pressure preferably lower than 10^{-3}–10^{-4} Pa. Then, a high purity working gas (desirably of 6 N purity) – often argon (Ar), due to its inertness, suitable atomic mass, and low cost compared to other inert gases – is introduced in the reactor chamber to achieve a typical gas pressure in the range of 0.1–1 Pa. The power source ionises the Ar gas atoms, rendering them positively charged. The electric field is produced between the negative cathode target and a nearby grounded anode, which can either be the magnetron own grounded anode shield or a grounded substrate, as shown in Fig. 1. The high energy Ar^+ species will be attracted and accelerated by the field towards the negatively charged cathode target. Ionised gas collides with the target material at high velocity, and if the delivered kinetic energy exceeds the binding energy of the target species, the constituting atoms will be ejected/sputtered across the reactor chamber, being collected at the substrate surface, positioned in the vicinity opposite to the cathode. The magnetic field created by magnetron cathode traps the electrons and other charged species near to the negatively charged target material, increasing the sputtering yield and maintaining the gas plasma discharge at low pressures. This feature nurtures larger mean free paths for the sputtered atoms, optimal for

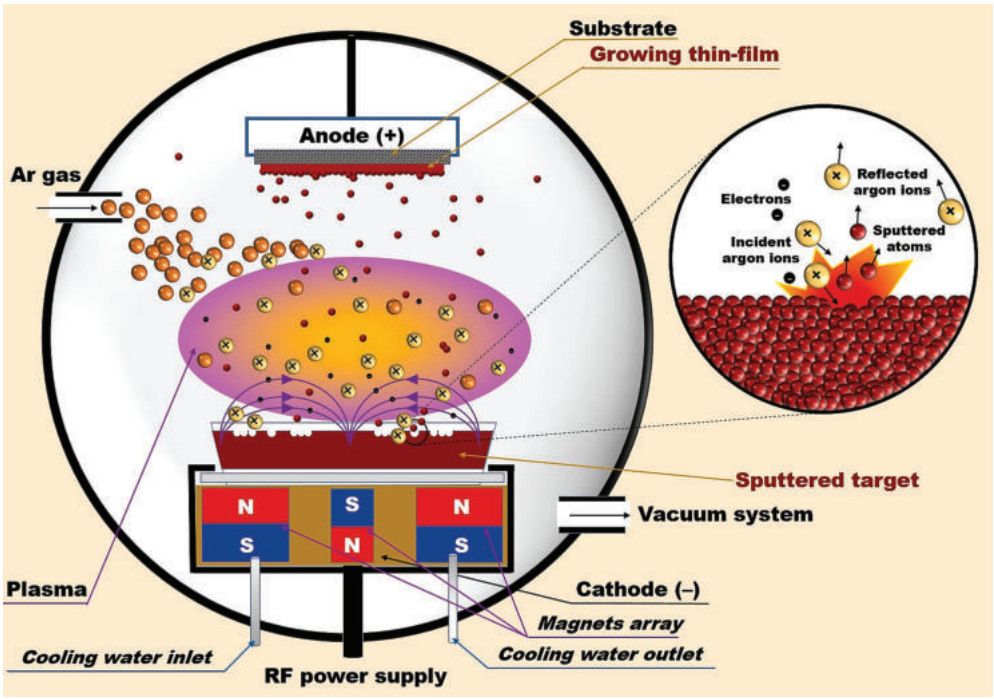

Fig. 1. An illustration of magnetron sputtering deposition process. Adapted after Ref. [75] and further completed.

preventing collisions (and loss of energy) between them and species present in the reactor chamber. The RF regime allows, by the alternatively change of polarity at high-frequency, to sustain the discharge and to circumvent the positive charge build-up at the target surface in the case of non-conductive materials. The build-up of charge on dielectric targets when trialling DC sputtering would otherwise inhibit any sputtering. Furthermore, reactive gases such as oxygen or nitrogen gas can be used in the production of thin-films of metal oxides or nitrides directly from metal cathode targets. Having already proven its usefulness in various industrial branches, RF-MS capacity to overcome technological limitations and easily scale up [67,73,74] should also promote its appeal in healthcare.

3. Magnetron sputtered bioactive glass films

Depending on their prominent type of network formers, BGs can be classified as silica- (SBGs), phosphate- (PBGs) and borate-based (BBGs) bioactive glasses [59]. However, in spite of all the RF-MS industrially-demonstrated performances, its successful application for single layer BG coating of endosseous implants (regardless if silica-, phosphate- or borate-based) was late to happen. The first recorded effort took place in 2003, when Mardare *et al.* [44] prepared silica-based bioactive glass (SBG) coatings on titanium (Ti) substrates, crystallized them in air at 900, 950 and 1000 °C, and only physical-chemically assessed them. Since then, major research efforts have been massively devoted by Stan & Ferreira on SBG thin-films (2009 – to date) [47,49,55,76–89] and by Stuart, Stan & Grant on phosphate-based bioactive glasses (PBGs) (2015 – to date) [50,90–95]. Solitary works, published by Bibby *et al.* (2005) [51], Slav *et al.* (2008) [46], Saino *et al.* (2010) [48] & Iijima *et al.* (2013,2014) [96,97] and Sato *et al.* (2020) [98] on SBGs and PBGs, respectively, could also be mentioned. Advanced research efforts have been put forward to disclose the key deposition factors of RF-MS sputtered SBG films, their biomineralization capability and biological performance. In contrast, the highly resorbable PBGs films have just recently reached a preliminary *in vitro* cytocompatibility testing stage [95]. Their attractive features, including the ability to rapidly and precisely release therapeutic ions (such as antimicrobials, like Ag and Ga, or osteogenics, like Ca or Mg) (Fig. 2), justify further attention from the scientific community. Sputtered BBGs have not been investigated yet, as only boron-doped SBG films were prepared to date [76,83,87,89].

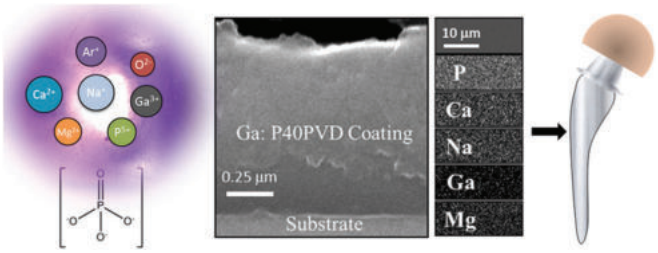

Fig. 2. Thin-film structures deposited by RF-MS from PBGs for releasing osteogenic (Ca, Mg, P) and antimicrobial (Ga) ions in orthopaedic implant applications. Reproduced with permission from Ref. [93].

3.1. Standalone silica-based bioactive BG coatings (of classical and innovative systems)

In 2003, Mardare *et al.* [44] published the first report on the RF-MS manufacture of SBG layers. They employed cathode target disks, fabricated by uniaxially pressing of a low-silica ($31.1SiO_2$–$31.75CaO$–$10.6P_2O_5$–$26.6MgO$ (mol%)) glass powder (grain size < 150 μm) prepared by melt-quenching (MQ), followed by sintering at 1200 °C – thus, a glass–ceramic target material. These as-sputtered films on Ti substrates had bond strength (pull-off) values of ~ 41 MPa. The films were then post-deposition heat-treated at 950 °C/30 min in air, and tested as such from physico-chemical, mechanical and *in vitro* biological (*i.e.*, apatite forming ability by immersion in Kokubo's simulated body fluid (SBF) [99]) standpoints. The amorphous glass films were successfully devitrified, with calcium magnesium phosphate ($Ca_7Mg_2P_6O_{24}$) and forsterite (Mg_2SiO_4) being the main crystalline phases. Scanning electron microscopy (SEM) analyses showed prominent cracks and titanium oxide crystals protruding through the coatings. Consequently, the adherence of the films to the substrate declined to ~ 16 MPa (close to the acceptable limit, *i.e.*, 15 MPa, imposed by the ISO 13779–2/2018 for HA

implant coatings [100]). Although not mentioned, this was a direct effect of the chosen extremely-high post-deposition annealing temperature, situated above the phase transformation temperature of Ti (*i.e.*, transition from the α-Ti hexagonal close packed phase to the β-Ti body-centred cubic one, taking place at 882 °C). This led to a decrease in the unit cell volume and thus, generating intense mechanical stresses. Such evidences might have unjustly suggested a limited capacity of RF-MS for producing high-quality SBG layers, and dissuaded, for some time, the scientific community interest. Nevertheless, signs of excellent biomineralisation capacity (*i.e.*, growth of a Ca-Mg-P rich phase on the surface of the SBG films) after just two days of immersion in SBF were highlighted.

Subsequently in 2005, Bibby *et al.* [51], again employed a MQ low-silica glass material ($29.6SiO_2$–$19.7CaO$–$21P_2O_5$–$19.7Al_2O_3$–$10.0CaF_2$ (mol%), Limerick Glass Company, product code LG112) as cathode target. The square target was manufactured by compressing the glass powder into a stainless-steel window frame mould, followed by sintering at 1000 °C/1h, resulting in a glass–ceramic which authors designated as of "*fluorapatite – mullite*" origin. No mention of a substrate heating during deposition or of post-deposition crystallization annealing treatments was made. Although the presence of crystallinity of the thin-films could not be measured by X-ray diffraction (XRD) (due to their thinness), such as-sputtered layers from complex oxide materials are expected to be amorphous/highly-disordered. This is due to the high activation energy for crystallization of the oxide glassy materials and the reduced transversal mobility of the (sputtered) adatoms under the low temperature deposition conditions (determining their "freezing" at the arrival sites) [67]. The RF-MS films had smooth/featureless surfaces. The glass-coated Ti6Al4V samples showed good cytocompatibility with MG63 human osteoblast cells (SEM microscopy evidences only), comparable to the one yielded by the uncoated metallic substrates. The cells mostly reached confluence after five days of culturing, while incipient cell mitosis was highlighted. However, instances of less-dense cell populations (while cells apparently still being well-spread and having a healthy shape) were noticed at the edges of the coated samples. Bibby *et al.* [51] issued two hypotheses: (*i*) either the BG coating had suboptimal adherence at the edges of the substrate; or (*ii*) the coating was damaged prior to biological testing during handling (which, one might add, still suggests of the coating's frailty).

The first results on SBG film deposition came from the National Institute of Materials Physics (NIMP), under the supervision of Dr. Constantin Moroșanu (who sadly departed in 2009, after losing his fight with an incurable disease), and were published in 2008 [46]. The 45S5-Bioglass® ($46.1SiO_2$–$26.9CaO$–$2.6P_2O_5$–$24.4Na_2O$ (mol%)) was here employed for the first time as source material for the RF-MS deposition of implant-type coatings. Furthermore, this was also the first time that a mildly-pressed (in a metallic shallow dish) glass powder was used as cathode target instead of compact variants (glasses directly melt-quenched into moulds/pre-forms, or compressed and sintered glass-ceramics disks). This simple, yet efficient approach, proved its great advantages, as it will be stressed later on. The RF-MS-derived 45S5 films had unusual rough surfaces, as evidenced by SEM. The highest used total sputtering pressure (*i.e.*, 0.7 Pa) and oxygen-in-argon dilution (*i.e.*, 15 vol%) led to the best target-to-substrate atomic transfer. Soon after (starting from 2009), Stan & Ferreira *et al.* concerted research efforts towards identifying solutions for improving the bonding strength of the SBG films [47,49,55,77,79,81,83,86,88,89], since poor adherence was considered the main obstacle hindering their load-bearing applications. The rather unique 1.78 MHz radio-frequency power source was used in the magnetron sputtering endeavours of Stan & Ferreira *et al.*, instead of the conventional 13.56 MHz one.

In the first attempt devoted to increasing the adherence of SBG films, a silica-rich alkali-poor SBG formulation ($58.5SiO_2$–$17.1CaO$–$4.5P_2O_5$–$7.9MgO$–$5.2Na_2O$–$6.8K_2O$ (mol%)), thus with a reduced coefficient of thermal expansion (CTE) with respect to 45S5 [101], was employed as cathode target in form of a simply "cold-pressed" non-sintered powder (into a metallic dish) [47]. The highest used working gas pressure (*i.e.*, 0.3 Pa) determined a better-quality target-to-substrate transfer of the chemical species within. The sub-micron films were investigated as-sputtered and post-deposition annealed at 550 and 750 °C in air (the latter ones were successfully devitrified, having $Na_2Mg(PO_3)_4$ as main crystalline phase). The FTIR spectroscopy showed similar absorption envelopes for the target and as-deposited and 550 °C-annealed films, denoting analogous structural features. The surface morphology of the as-deposited and 550 °C-annealed coatings was rather homogenous and defect-free. In the case of the 750 °C-annealed samples, the combined SEM, energy dispersive X-ray spectroscopy (EDXS) and XRD analyses, evidenced the formation of TiO_2-rutile in form of crystals, which evolved through the SBG film towards its surface, and "exploded" in form of rivets-like formations in contact with the oxygen-rich air ambient. Still, no micro-cracks were revealed. The remarkable pull-off adherence values obtained for the as-deposited and 550 °C-annealed coatings (with the fracturing occurring in the glue volume at values of ~ 85 MPa) could be ascribed to the high-silica glass composition and to the intense argon ion plasma etching process (10 min, DC bias voltage of 0.4 kV, electric power of ~ 200 W) of the substrate prior to deposition (*via* a W-filament plasmatron). This pre-deposition treatment was aimed to remove oxide layers and other residual impurities and activate the substrate surface. The adherence values are the highest reported to date for SBG coatings. Unexpectedly, considering their piercing by TiO_2 crystals (known to have a deleterious effect on adherence [44]), the 750 °C-annealed SBG coatings still yielded noteworthy bonding strengths of ~ 73 MPa. This could have been determined by the pre-deposition substrate etching step and a chemical bonding (by inter-diffusion) between the coating and the substrate, as a perovskite ($CaTiO_3$) phase was evidenced to form by XRD. However, both the as-deposited (glass) and the 700 °C-annealed (glass–ceramic) films proved insoluble and thus, bioinert, upon immersion for 30 days in SBF [85].

The next studies performed by Stan *et al.* in 2010 were oriented towards the deposition, mechanical testing and *in vitro* biological assessment of RF-MS films of the celebrated and clinically approved 45S5-Bioglass® formulation [84–86,88]. The same concept of "cold" mildly-pressed powder targets was employed. Again, the higher employed argon sputtering pressures (between 0.3 and 0.45 Pa) fostered improved replication of the source cathode target complex stoichiometry [84–86]. The CTE of 45S5-Bioglass®, of ~ 15×10^{-6} °C^{-1} [101], is significantly higher with respect to Ti and its medical-grade alloys (~8.6–9.8 × 10^{-6} °C^{-1}) [102–104]. The performed experiments showed rather low bonding strengths (pull-off) for the simple 45S5-derived sub-micron-thick films. It was thus suggested that the pre-deposition Ar ion plasma etching step of the substrate, could not fully compensate the (*i*) large CTE mismatch between the deposited films and the Ti-based substrate and (*ii*) stresses generated at the temperature reached by the substrate during deposition (*i.e.*, ~150 °C) [88]. The remedy technical solution consisted of (*a*) depositing of a ~ 70 nm-thick buffer layer with compositional gradient (*i.e.*, SBG_xTi_{1-x} (x = 0–1)) at the Ti substrate–SBG coating interface (by co-sputtering from two targets, at the same power density, while continuously rotating and translating the substrate holder between the two Ti and SBG 90°-distanced cathodes, positioned on the circumference of the spherical reactor chamber (Fig. 3); (*b*) followed by post-deposition annealing treatments performed at 650–700 °C/2h in air [86,88]. Titanium oxide aggregates were observed by SEM on the surface of the simple (abrupt) post-deposition annealed SBG/Ti films. This led to SBG layer peel-offs (with diameters of ~ 20–40 μm), occupying a total area of ~ 15% from the total film surface [86]. The annealed graded SBG/SBG_xTi_{1-x}/Ti films were more homogeneous, showing little-to-no exfoliations or micro-cracks and suggesting that the compositionally graded buffer layer attenuated the abrupt interface of the dissimilar materials and increased their bonding strength [86]. Indeed, the pull-off measurements performed in a subsequent study [88], indicated a ~ 1.7 times improvement of the bonding strength of the graded SBG/SBG_xTi_{1-x}/Ti films (~50 MPa) with respect

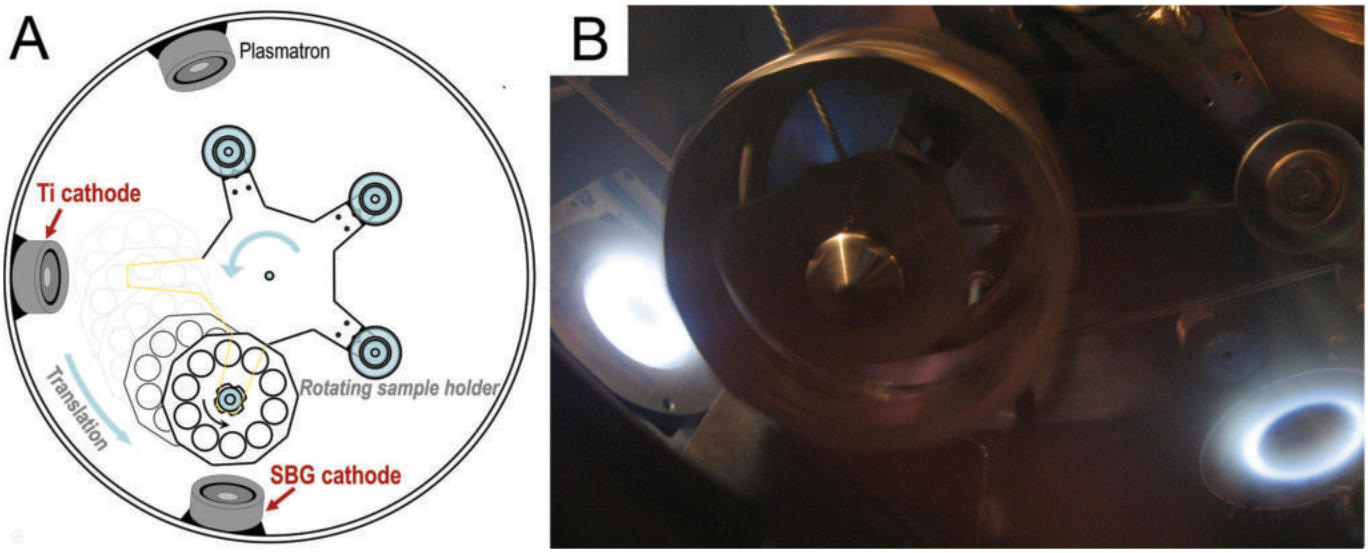

Fig. 3. (A) Schematic representation of the compositionally graded SBG_xTi_{1-x} (x = 0–1) buffer layer by magnetron co-sputtering. Reproduced and adapted with permission from Ref. [108]; (B) Snapshot taken during the process of the compositionally graded SBG_xTi_{1-x} (x = 0–1) buffer layer.

to the abrupt SBG/Ti ones (~29 MPa). The SBF *in vitro* testing of the annealed 45S5-sputtered films (having combeite-$Na_4Ca_4Si_6O_{18}$, Na_3PO_4, and wollastonite-$CaSiO_3$ as main crystalline phases) indicated that they generally abided the apatite formation mechanism proposed by L.L. Hench [105], showing after (*i*) 3 days the formation of the silica-rich layer (prerequisite for the formation of apatite-like ingrowths), with H^+ migration to form Si–OH^- bonds and the repolymerisation of the surface silica suggested to be simultaneous processes [84]; and (*ii*) 30 days the formation of fully-developed apatite-like layer [85]. The as-sputtered amorphous 45S5 films were completely dissolved after 30 days of immersion, confirming their high resorbability due to the large alkali content [85]. The "burst release" of sodium (Na) from the 45S5 glass and the linked pH increase are now well-known issues, which can led to less than optimal biological responses (including cytocompatibility) [106,107]. The implementation of a preconditioning (Na leaching) step in various synthetic physiological fluid variants of (*e.g.*, Tris buffer, SBF or cell culture media) was proposed to reduce these undesirable phenomena [106,107]. In the Stan *et al.* [88] study on the 45S5 sputtered coatings, it was shown that the innate poor stability of the as-deposited layers in physiological fluids can be tailored by devitrification heat-treatments, aiming to improved biological performance outcomes. Furthermore, the annealed 45S5 sputtered coatings showed good cell adhesion and viability, as well as cell proliferation capacity, when tested in human primary osteoblasts (hOB) cell cultures derived by the differentiation of human mesenchymal stem cells isolated from bone marrow aspirates [88].

Two more supplementary reports in the field of 45S5 magnetron sputtering coatings were later (2013 & 2014) published by Iijima *et al.* [96,97]. Interestingly, they have employed [96,97] the same type of cold-pressed MQ powder targets that were earlier (2008–2012) introduced by Slav *et al.* [46] and Stan *et al.* [47,76,83–89]. Their research aimed at bio-functionalizing alumina implants with SBG coatings for dentistry applications. No information on the composition and structure of the films was provided [96]. The formation of calcium phosphate deposits was noticed on the surface of the 45S5-coated alumina specimens submerged in artificial saliva for 6 months, advocating for the biomineralisation capacity of the coatings. In their second study [97], the ability of SBG coatings deposited on alumina on the recovery of the mechanical properties of the etched enamel by remineralisation processes was successfully confirmed (*via in vitro* assays performed in artificial saliva).

In 2010, Saino *et al.* [48] used a sol–gel 58S (59.8SiO_2–38.5CaO–1.7P_2O_5 (mol%)) glass powder as a target for coating 3D Ti6Al4V macroporous (square pores with sizes of ~ 800 μm) by RF-MS. They have employed a 3-cathode gun confocal system (with the guns tilted at 30°) for increased deposition rates and (probably) improving of the out-of-sight deposition, benefiting from off-axis sputtered atom fluxes. No mention of this RF-MS configuration ability to coat inside the macroporous scaffold was made. Complex *in vitro* testing in human osteosarcoma (SaoS-2) cell cultures were performed. Remarkably, the SBG-coated Ti6Al4V scaffolds outperformed the uncoated counterparts, leading to a (*i*) two-fold increase in cell proliferation, alkaline phosphatase activity, and mineralisation; and (*ii*) enhanced deposition of important extracellular matrix proteins (*i.e.*, decorin, fibronectin, osteocalcin, osteonectin, osteopontin, collagen type I, and collagen type III) – promising traits for boosting the osteointegration and fixation rate, and thus, shortening of healing time.

In the third attempt devoted to increasing the bonding strength of SBG films, two alkali-poor, boron and/or fluorine doped MQ SBG formulations, with low CTEs, were employed as powder targets in the RF-MS experiments: *i.e.*, 1b (39.9SiO_2–31.0CaO–2.6P_2O_5–13.3MgO–4.4Na_2O–4.4B_2O_3–4.4CaF_2 (mol%), CTE = 10.7×10^{-6} °C^{-1}) [109,110] and 1d (45.5SiO_2–30.3CaO–2.6P_2O_5–13.0MgO–4.3Na_2O–4.3CaF_2 (mol %), CTE = 10.4×10^{-6} °C^{-1}) [110].

Compositional differences between the source target material and sputtered 1b SBG films (2010–2012) were noticed, being consistent with the standard free energy of the oxidation reactions of the different elements involved [109,110]. Such findings disclosed the remarkable possibility to derive a plethora of film compositions from a single target formulation by the simple modification of the sputtering total pressure and oxygen-to-argon dilution [76,83,87,89]. Moreover, good bonding strength (pull-off) values were obtained for the 1b-derived SBG thin-films, in the range of ~ 45–73 MPa [89]. Grazing incidence XRD, Fourier transform infra-red (FTIR) spectroscopy, EDXS, and SEM coupled analyses evidenced continuous morpho-structural and compositional changes taking place at the surface of the originally sub-micron thick SBG films, upon immersion in SBF, culminating with the formation (after 30 days of soaking) of > 1 μm thick homogenous layer of a crystalline carbonated hydroxyapatite (CHA). The CHA layer consisted of spherulitic aggregates composed of fine acicular crystallites (Fig. 4), testimony of an excellent biomineralisation capability [111]. The CHA growth mechanism seemingly relies on heterogenous nucleation [76], determined by electrostatic interactions between the negatively charged (Si–OH^- rich) surface of the SBG thin-film and the cations, and then

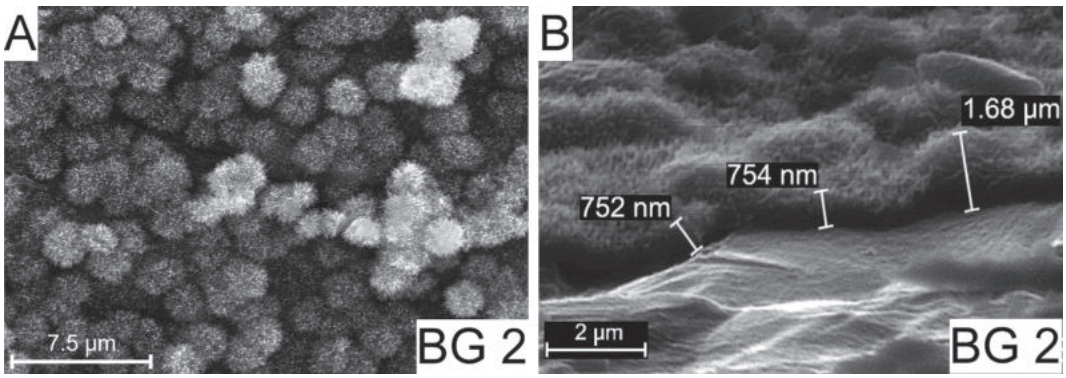

Fig. 4. (A) Top-view and (B) tilt-view SEM images of 1b-derived SBG films immersed for 30 days in SBF at 37 °C. Reproduced with permission from Ref. [83].

anions from the SBF solution, since the supersaturation of the SBF medium is highly unlikely due to the very low film mass/SBF volume ratio (when abiding the ISO 23317/2014 currently in effect [112]).

In 2013, Stan *et al.* [49] revisited the RF-MS deposition of the SBG formulation employed by Mardare *et al.* [44] in their 2003 research (*i.e.*, 31.1SiO_2–31.75CaO–10.6P_2O_5–26.6MgO (mol%)). This time, the films were post-deposition heat-treated in air at a lower temperature of 750 °C (slightly above T_g (716 °C) of this glass), therefore, below the α → β phase transition point of the Ti substrate material. Low thickness (*i.e.*, ~360–450 nm) films were preferred to facilitate the atomic inter-diffusion investigations. The moderate annealing temperature provided the required energy for atomic inter-diffusion phenomena to take place at the SBG/Ti interface. This was demonstrated by the formation of inter-metallic TiSi, Ti_5Si_4, and Ti_5Si_3 phases, which greatly increased the interfacial bonding strength of the SBG films from ~ 38 MPa (as-deposited) to ~ 60 MPa (750 °C-annealed). It was hypothesized that the nucleation of the Ti_xSi_y phases could also be stimulated by the presence of an intermixing Ti–Si thin layer generated by ballistic implantation of Si atoms into Ti substrate surface/sub-surface when working at low target-to-substrate distances. The atomic inter-diffusion phenomena were not unique to this specific SBG target formulation, as similar events were evidenced also for the 1b and 1d SBG compositions [49].

In the framework of 1d SBG (45.5SiO_2–30.3CaO–2.6P_2O_5–13.0MgO–4.3Na_2O–4.3CaF_2 (mol%)) studies (2014–2016), the first efforts were devoted to the adaptation of the deposition conditions (markedly the deposition pressure and the oxygen-in-argon dilution) in search for RF-MS regimes which could foster joint good (*i*) mechanical and (*ii*) cytocompatibility performances. Overall, the most suitable operating conditions were a sputtering pressure of 0.4 Pa and an inert (Ar) working atmosphere [77,78]. Such 1d-derived SBG films enjoyed the best: (*i*) values of pull-off adherence (~63 MPa, higher than the FDA limit of ~ 51 MPa [14]), hardness (H≈5.7 GPa), and elastic modulus (E≈77 GPa), thus, H and E similar to the plasma sprayed commercial HA implant coatings and dental enamel, and higher with respect to cortical bone; and (*ii*) cytocompatibility responses in mouse fibroblast NIH/3T3 cell cultures [77]. The encouraging results endorsed the application of the optimized SBF RF-MS recipe for the coating of real dental implants with ~ 1 µm-thick layers [55]. The "line-of-sight" deposition difficulties of RF-MS were surpassed by fixing the dental implants parallel to the cathode target surface and continuously rotating them during sputtering with the help of a vacuum stepper motor (Fig. 5A,B). The bonding strength of the coating to the implant surface is of critical importance for clinical efficacy of such medical systems. Even if the results of static mechanical tests were promising [77], the authors considered that the "cold implantation" of the SBG-coated dental screws in cadaveric pig mandibular bone, followed by tension-free extraction tests, will provide a more accurate account of their performance since they will be subjected to the complex mechanical stresses occurring upon implantation by screwing (Fig. 5C). The multiple-site SEM and EDXS analyses indicated that the bonding strength between the SBG and the Ti-based dental screws is quite strong, as no delamination or cracks were noticed, only compacted sections in the thread areas of the implants (consequence of reaming the hard bone tissue during screwing) being scarcely revealed. The *in vitro* cytocompatibility assays showed that 1d-derived SBG films led to the good adhesion and proliferation of human dental pulp stem cells (hDPSCs), and allowed for the conservation of the undifferentiated phenotype of the hDPSCs, which were able to give birth to spherical stem cells colonies (Fig. 5D,E) [55]. The conservation of the stem cell pool is vital for the health of the *peri*-implant structures, since this will provide in time the necessary osteoblast number. If the stem differentiation will be triggered by cell signalling processes alone, this could prolong the life of dental implants, tentatively eliminating the necessity of further surgical interventions.

In another 1d-based SBG research [78], the growth of sub-micrometre hollow cone-shaped needles by RF-MS was demonstrated (Fig. 6A,B), in the absence of any template or catalyst. Their fabrication, non-specific to this particular SBG formulation, takes advantage of the self-shadowing mechanisms (characteristic to RF-MS processes occurring at low deposition temperatures); almost instantaneous condensation of vapour species, with low transverse mobility of the adatoms; and asymmetric oxidation of the peaks and valleys of roughened Ti substrate [78]. The structure-controlled degradation in blood plasma and the excellent cytocompatibility in human umbilical endothelial vein (HUVEC) cell cultures was shown [78]. Such resorbable sub-micrometre hollow cone-shaped needles of SBG can be envisaged as medical devices for focal transient permeabilization of the blood–brain barrier (BBB) – known to be impervious toward many drugs which can lead to resistance in the treatment of carcinoma and neurodegenerative disorders [78].

SBG films were applied also on biodegradable Mg-based alloys (*i.e.*, Mg-0.8Ca), aiming to reduce their corrosion rates [79,82]. Two SBG formulations were used, one with conventional silica content (42.3SiO_2–24.2CaO–2.0P_2O_5–22.4MgO–9.1Na_2O (mol%)) and one with high silica content (55.3SiO_2–20.5CaO–1.6P_2O_5–17.1MgO–5.5Na_2O (mol%)) [79]. Their compositions were well-reproduced into coatings using an argon deposition pressure of 0.4 Pa, and a long pre-sputtering time (45 min). Similar interfacial adherence values were inferred for the SBG/Mg alloy samples, of ~ 28–33 MPa [79], thereby, inferior to those typically obtained for the SBG/Ti joints. The silica-rich SBG films were advanced for further biological and corrosion testing, and compared to crystalline CHA films (of similar thickness) deposited by RF-MS as well [82]. The *in vitro* cytocompatibility response of the silica-rich SBG films was similar or even marginally superior to crystalline CHA counterparts, when tested up to 72 h in human fibroblast (Hs27) and osteosarcoma (Saos-2) cell cultures [82]. The SBG films reduced the weight loss and the hydrogen release rate of the Mg-based substrate, and improved its corrosion response (in SBF and cell culture Dulbecco's Modified Eagle Medium (DMEM)), yielding a more electropositive corrosion potential, a lower corrosion current density, and a higher polarization resistance.

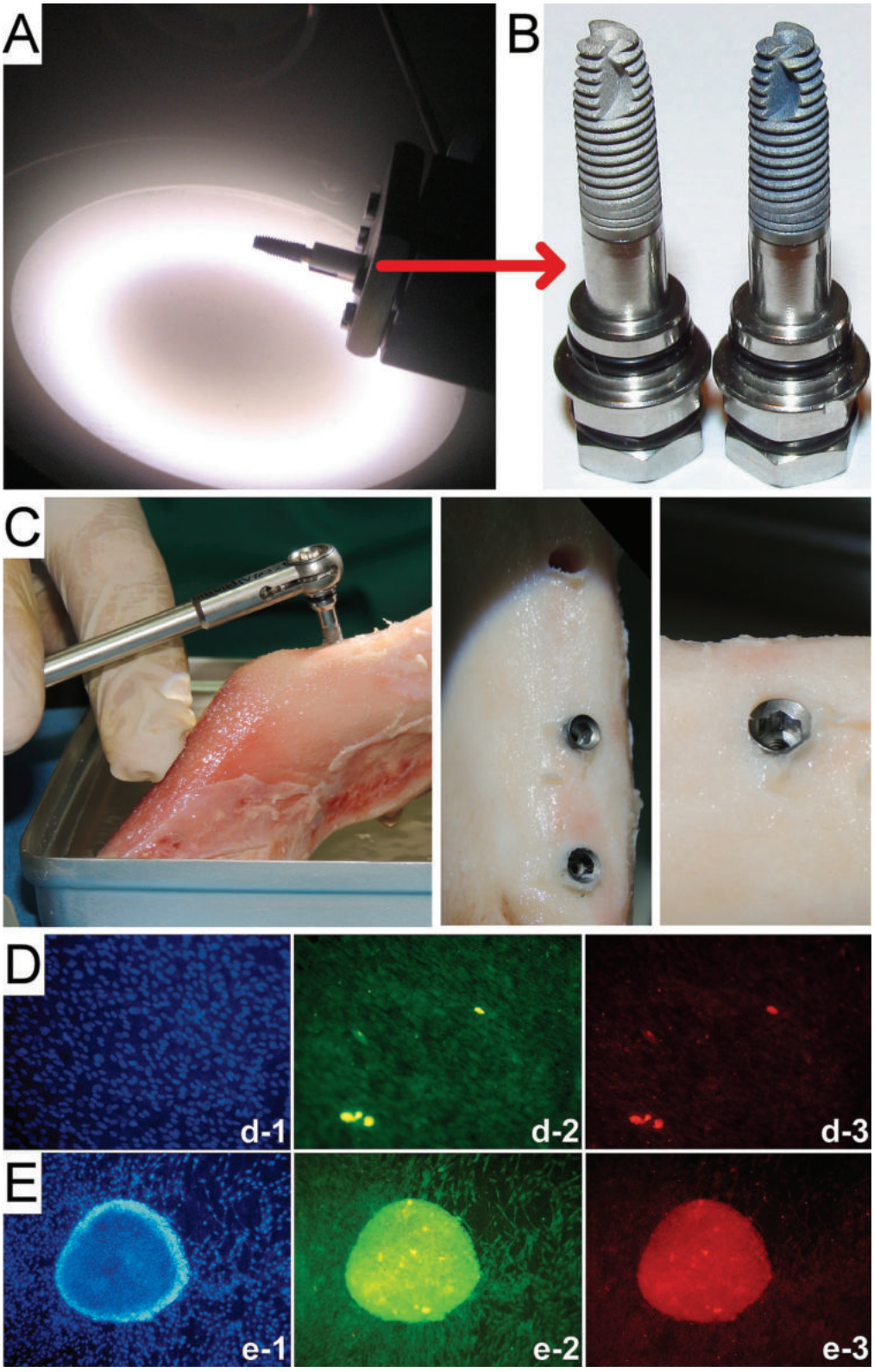

Fig. 5. (A) Snapshot taken during the RF-MS coating process of a dental screw with 1d SBG. (B) Comparative images of simple (left-hand side) and SBG functionalized (right-hand side) Alpha-Bio® DFI dental implants. (C) Representative images acquired during the implantation-extraction procedure of the dental screws biofunctionalized by RF-MS with 1d-derived SBG coatings. (D, E) Indirect immunofluorescence images presenting hDPSCs grown on the (D) bare Ti substrates and (D) as-deposited 1d-derived BG films, after 10 days after seeding. cells nuclei (in blue – d-1, e-1); CD90 expression of cells (in green – d-2, e-2); and STRO1 expression of cells (in red – d-3, e-3). Objective. 20 × for (D) images and 10× (E) images. Reproduced with permission from Ref. [55]. (For interpretation of the references to colour in this figure legend, the reader is referred to the web version of this article.)

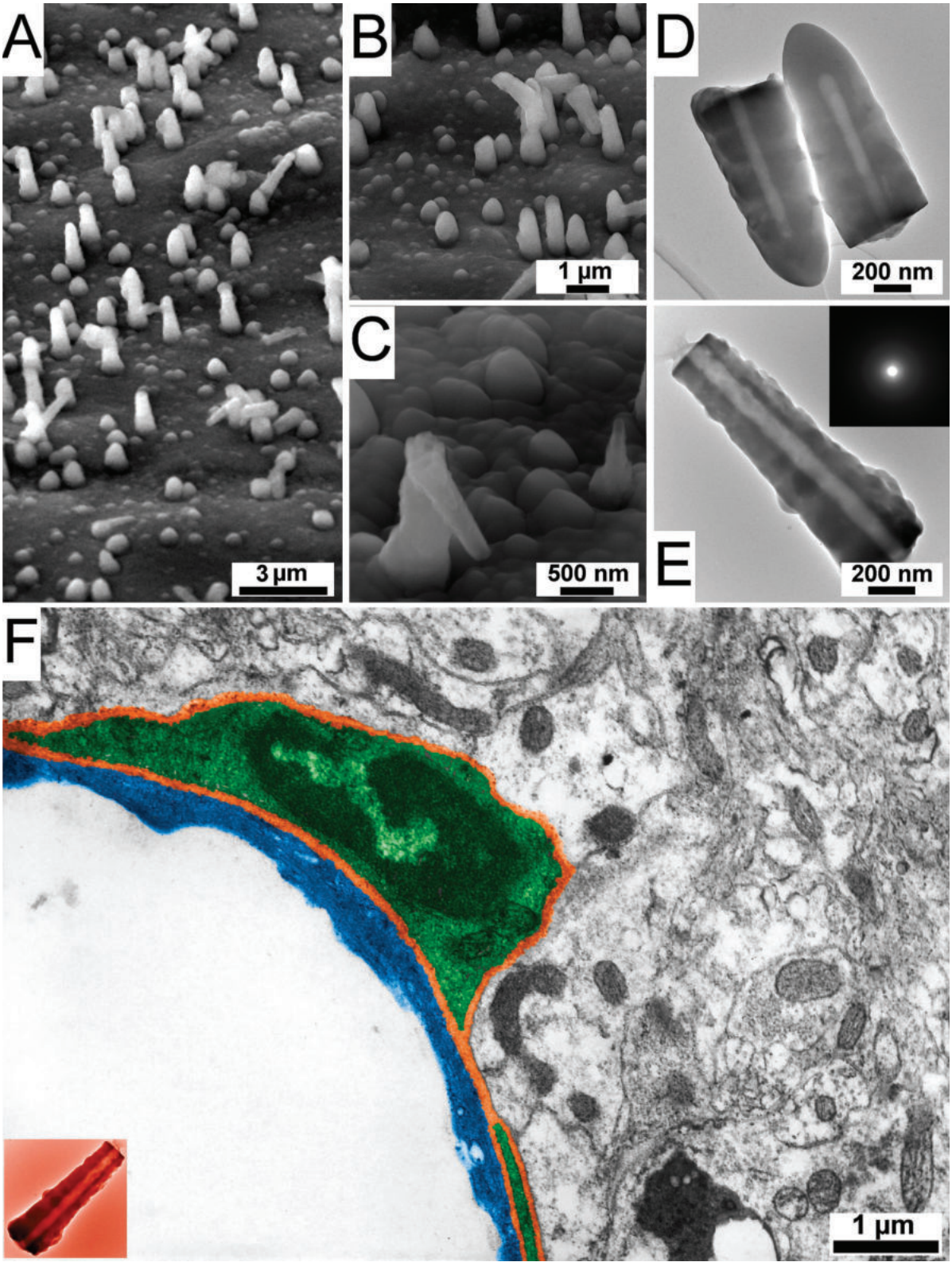

Fig. 6. (A–C) SEM images of the 1d-based grown by RF-MS on the surface of Ti substrates. (D,E) TEM images of hollow sub-micrometre cones collected for the 1d-based SBG coating deposited at a sputtering argon pressure of 0.4 Pa. Inset of (E): SAED pattern for one SBG cone. (F) TEM image of normal rat brain (magnification 22,000×): (bottom left) the lumen of the capillary, the BBB (pseudo-coloured in blue), the basal membrane of the capillary (pseudo-coloured in orange), a pericyte in a pouch of the basal membrane (pseudo-coloured in green), and the brain tissue with fragments of neuronal and glial cells and the intercellular space (native grey scale). Inset: a TEM image of a sub-micrometre hollow cone (pseudo-coloured in red) at the same magnification (hence, using the same dimensional scale) as the brain tissue, envisaged a potential healthcare application. Reproduced with permission from Ref. [78]. (For interpretation of the references to colour in this figure legend, the reader is referred to the web version of this article.)

Nevertheless, overall, the corrosion performance of SBG layers was lower than that conferred by the crystalline CHA coatings.

Recently, there has been a focus on triggering special features in glasses by incorporating ions with better osteointegration and additional biological functionalities (*e.g.*, angiogenesis; antitumoral activity; antimicrobial effect) [59,113]. In congruence to these new advances, efforts have been devoted to delineate new glass compositions with reduced CTEs [114] and augmented antimicrobial effects (by combining antimicrobial agents with different antimicrobial action mechanisms, *i.e.*, Zn, Sr, Cu, Ga) [114,115]), optimal for the development of a new generation of RF-MS-based BG coatings. Thereby, the newest RF-MS deposition researches (2017 – to date) were focused on alkali-free SBG systems (single- or double-doped with Zn/Sr or Cu/Ga) [80,81], derived from the FastOs®BG system ($38.5SiO_2$–$36.1CaO$–$5.6P_2O_5$–$19.2MgO$–$0.6CaF_2$ (mol%)), known for its fast biomineralization capacity in SBF and demonstrated *in vivo* (on animal model) osteointegration properties [114,116,117].

Popa *et al.* [80] employed a Zn-doped FastOs®BG (*i.e.*, Z4S0: $38.5SiO_2$–$36.1CaO$–$5.6P_2O_5$–$15.2MgO$–$4.0ZnO$–$0.6CaF_2$ (mol%)) and deposited series of SBG coatings with intentionally increased silica-contents (*via* co-sputtering from SBG and fused silica) to tailor network connectivity that governs the dissolution rate and biomineralisation capacity of SBGs. These were used as a reliable platform for assessing the role of the increasing degree of mimicry of the synthetic physiological testing fluids on the apatite-forming ability. Films with (*i*) good replication (Fig. 7A) of the composition and structure of the source (cathode target) material (due to the increased pre-sputtering time) and (*ii*) gradually increased degree of connectivity (by co-sputtering) were successfully fabricated (Fig. 7A). All SBG films exhibited smooth morphologies typical to RF-MS (Fig. 7B). The testing media were: inorganic SBF and organic–inorganic DMEM (type D8437), simple and supplemented with 10% foetal bovine serum (FBS), under normal atmosphere (as the ISO 23317/2014 [112] seems to suggest) and under the correct homeostatic conditions (humidified atmosphere and 5 kPa CO_2). The

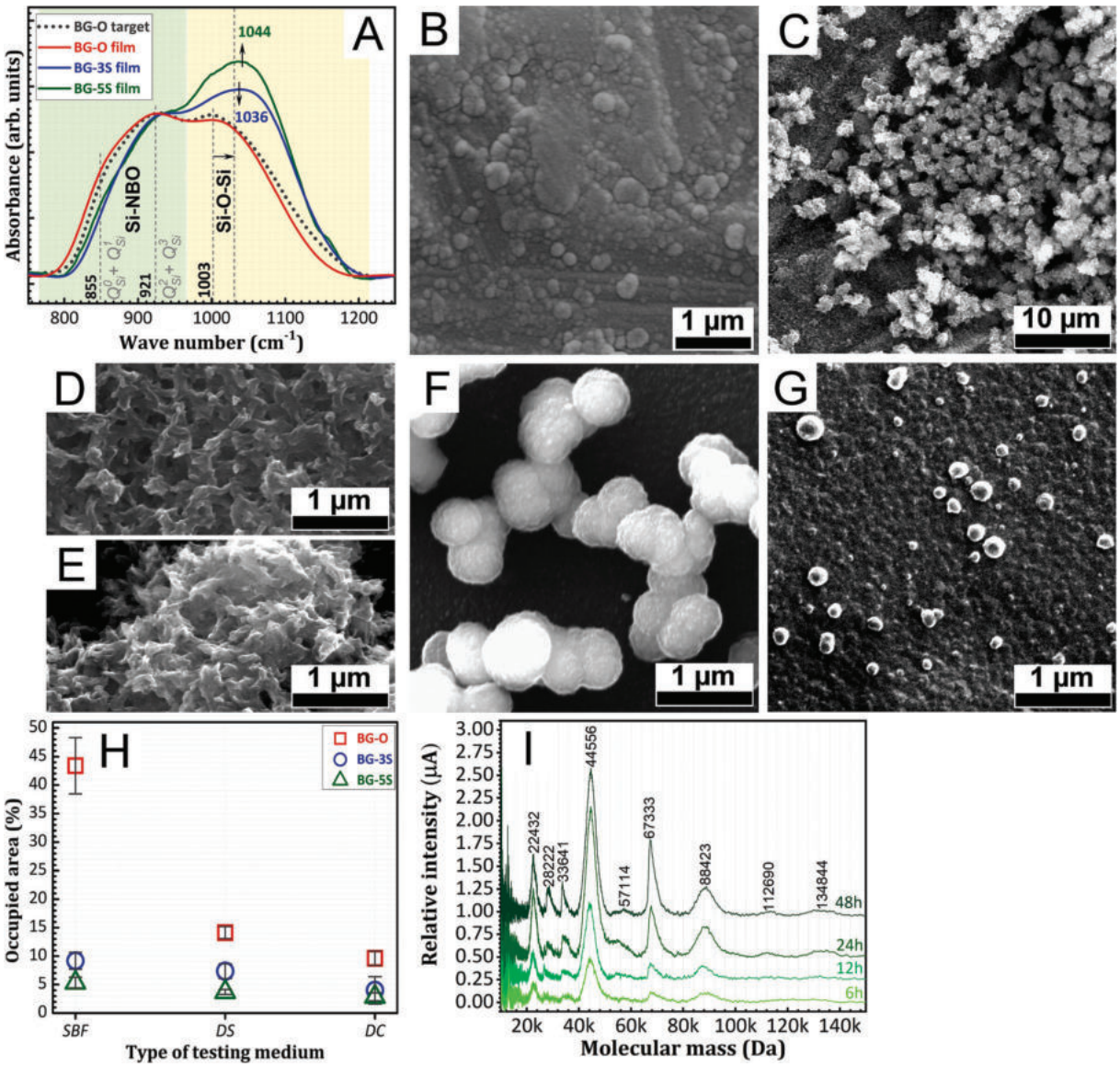

Fig. 7. (A) Comparative FTIR spectra of the Z4S0 cathode target and RF-MS films with increasing contents of silica (BG-O < BG-3S < BG-5S). (B) Typical SEM surface morphology of the as-sputtered SBG films; Surface morphology of the films immersed *in vitro* for 28 days in (C–E) SBF, (F) simple DMEM (DS), and (G) DMEM-10% FBS (DC); (H) Comparative representation of average areas occupied by the calcium phosphate aggregates/nodules deposited *in vitro* in SBF, simple DMEM (DS), and DMEM-10%FBS (DC) media, in the case of the SBG films with increasing silica content; (I) SELDI-ToF spectra of proteins adsorbed on BG-O film incubated for 6, 12, 24, and 48 h in the DMEM-10%FBS (DC) solution. Adapted after Ref. [80] – International Journal of NanoMedicine 2017:12 683–707 – Originally published by and used with permission from Dove Medical Press Ltd.

increase in the network connectivity of the SBG films had the expected effect of decreasing the CHA growth speed, regardless of the type of testing medium. The increase of the biomimicry of the apatite-forming ability protocol (in terms of both medium composition and testing ambient) led to a remission of the CHA development, from a well-crystallized rough matrix composed of intertwining fine acicular crystals on the top of which full-fledged micro-sized spheroid particulates (in SBF), down to isolated sub-micron-sized spherical nodules of CaP nature (Fig. 7C–G), but with a lower degree of ordering (in DMEM-10%FBS). The relative extent of biomineralization was inferred based on systematic microscopy studies, quantifying the area occupied by the spheroid aggregates/nodules (Fig. 7H). The deceleration of biomineralization in the presence of organic moieties (*i.e.*, amino acids and/or proteins) was highlighted. This is owned to the (*i*) lower pH attained with the increase of compositional biomimicry of the testing medium (close or similar to the physiological pH) and (*ii*) formation of a protein-based "screening" layer (as revealed by surface-enhanced laser desorption/ionization time-of-flight mass spectrometry (SELDI-ToF) investigations (Fig. 7I)), which retarded the bioactivity processes. The authors stressed that although the apatite-forming ability (evaluated using SBF assays) can be considered as valid indicator, the speed with which these processes occur cannot be translated to real biological conditions. This needs to be underlined, since there seems to be an inclination for evaluating the bonding capacity of SBGs to the neighbouring (hard and soft) living tissues by the temporal interval needed to induce the CHA growth in SBF. All SBG films shown excellent cytocompatibility in mesenchymal stem cell cultures. Further, technical proposals aiming for the unification of the apatite-forming ability protocols (possibly extending to the *in vitro* degradation, ion-release, and corrosion tests) for samples with different forms and dimensions (bulk objects, powders, scaffolds, thick coatings, and now, *thin-films*) were advanced [80], in continuation of Maçon *et al.* suggestions [118]. An appeal for more exigent and standardised *in vitro* assays was made, since only this desiderate can sieve the best SBG formulations and fast-forward their translation to clinic.

Furthermore, undoped and Cu & Ga doped RF-MS SBG films [81], with intentionally increased silica content (and thus, higher network connectivity) were derived from FastOs®BG and C2G3 ($38.5SiO_2$–$34.1CaO$–$5.6P_2O_5$–$16.2MgO$–$2.0CuO$–$3Ga_2O_3$–$0.6CaF_2$ (mol%)) formulations by co-sputtering. Improved mechanical properties and moderated solubility were aimed for. The Cu and Ga co-doped SBG films were slightly more polymerized than the undoped ones. Furthermore, the incorporation Cu and Ga led to a minor increase in hardness (from ~ 5.8 to ~ 6.1 GPa) and critical load of scratch delamination (from ~ 4.3 to ~ 4.9 N) and decrease in elastic modulus (from ~ 136 to 127 GPa) [81]. Furthermore, a majorly improved wear resistance performance with respect to both bare and undoped SBG coated substrates (Fig. 8A–D) was obtained [81]. Both types of films had noteworthy bonding strengths (pull-off) (of ~ 54 MPa) and good cell proliferation in mouse fibroblast (NIH/3T3) cell cultures. Remarkably, the Cu and Ga co-doped SBG films induced a pronounced antibacterial effect against the *Staphylococcus aureus* strain (after 24 h), reducing its growth by ~ 4 orders of magnitude with respect to the control situations (*i.e.*, the nutritive broth and the bare Ti substrate) [81].

The compositions of SBG targets, the types of substrates, the RF-MS parameters and the main outputs of the performed studies are summarized in Table 1.

3.2. Composite coatings

Besides the efforts devoted to manufacture single (individual) layers of SBG, which were the focus of this review work, the scientific literature also records the deposition of composite coatings encompassing silicate glasses. The first example concerns the class of HA-SBG blended coatings [45,54,56,119,120]. Due to their compositional intricacy and assorted joint contribution of dissimilar materials such data cannot be put in direct comparison with the standalone SBG coatings. More precisely, in the period (2005–2016), the group led by J.A. Jansen, one of the worldwide pioneers of the HA deposition by RF-MS [121,122], synthesized and biologically tested mostly HA-SBG blended layers [45,54,56,119,120]. They employed as SBG the commercially available S53P4-BonAlive® system ($53.8SiO_2$–$21.8CaO$–$1.7P_2O_5$–$22.7Na_2O$ (mol %)). In only two instances, SBG coatings were analysed standalone [45,119]. First, the as-deposited ~ 1 μm-thick SBG films were reported to dissolve completely in SBF within a period of 4 weeks [45]. In the next study, the 550 °C heat-treated BG films (so, probably partially crystallized) were outperformed by the 600 °C heat-treated HA ones when tested in rat bone marrow cell cultures [119]. The authors linked this to the "*instability of the BG coatings*". Except for the power (*i.e.*, 100 W), no information on the sputtering parameters employed in the deposition of the SBG and HA-SBG films was provided [45,119]. Next Jansen & van

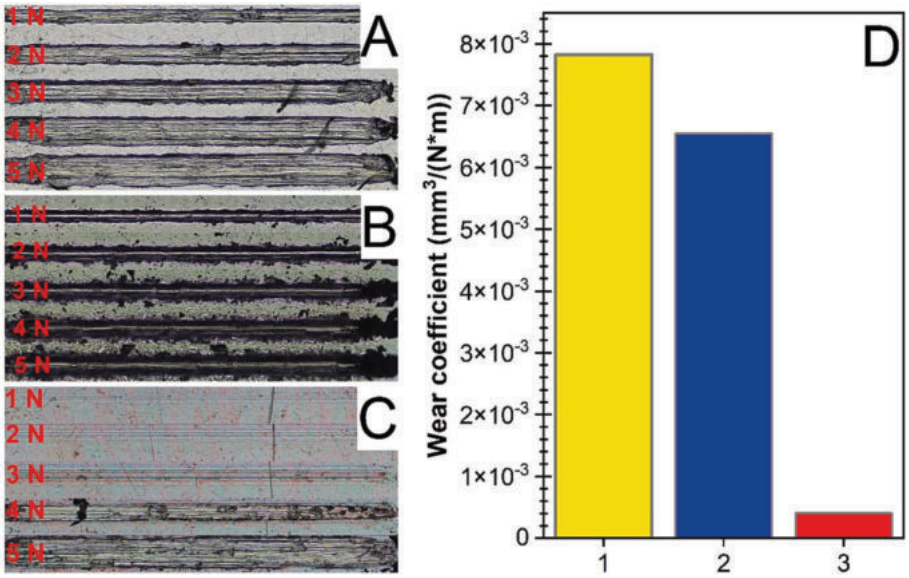

Fig. 8. Optical microscopy images of the wear tracks recorded at five incremental load values (*i.e.*, 1, 2, 3, 4 and 5 N), with 10 passes per load at a displacement rate of 4 mm/min, in the case of the (A) bare Ti and the (B) silica-enriched FastOs®BG- and (C) Cu&Ga-FastOs®BG-coatings. (D) The wear coefficient under the load of 5 N: (1) bare and silica-rich (2) FastOs®BG and (3) Cu&Ga-FastOs®BG coated Ti substrate. Reproduced with permission from Ref. [81].

Table 1
The main results of depositing various single layer SBGs by RF-MS onto different substrates.

Cathode target SBG composition (mol%)	Substrate	RF-MS parameters	Main results	Refs.
31.1SiO_2–31.7CaO–10.6P_2O_5–26.6MgO	• pure Ti • Ti coated Si/SiO_2	• Target diameter: 50.8 mm • Target type: 1200 °C sintered compact disk of compressed MQ glass powder • Driving radio-frequency: *not mentioned* (probably, 13.56 MHz) • Target-to-substrate distance: *not mentioned* • Electrical powder: 100 W • Sputtering gas: Ar • Sputtering pressure: 1 Pa • Status: as-deposited & post-deposition heat-treated at 950 °C/30 min in air	• Film thicknesses: ~ 360 nm; • Deposition rate: ~ 2.9 nm/min; • Use of electrical higher electrical powder of 150 W damages the compact glass cathode target;-The as-sputtered layers yielded bonding strength (pull-off) values of ~ 41 MPa; • The films crystallized at 950 °C (well-above the α → β transition point of Ti), had SEM-noticeable cracks, which led to a significant decrease in bonding strength down to ~ 16 MPa; • Early biomineralisation signs were noticed after being soaked for just two days in SBF.	[44]
	• pure Ti • Si	• Target diameter: 110 mm • Target type: mildly-pressed MQ powder at RT (grain size < 25 μm), NO sintering • Driving radio-frequency: 1.78 MHz • Target-to-substrate distance: 35 & 55 mm • Electrical powder: ~100 W • Sputtering gas: Ar • Sputtering pressure: 0.4 Pa • Status: as-deposited & post-deposition heat-treated at 750 °C/2h in air	• Film thicknesses: ~ 360–450 nm; • Deposition rate: ~ 6 – 7.5 nm/min (decreasing with the increase of the target-to-substrate separation distance); • The selection of an annealing temperature situated in the vicinity of the T_g (*i.e.*, 750 °C), enabled atomic inter-diffusion phenomena at the SBG – Ti interface, resulting in formation of Ti_xSi_y intermetallic crystalline phases with beneficial effects on bonding strength; • In the best case, a ~ 57% increase in adherence of the SBG thin-films was recorded.	[49]
29.6SiO_2–19.7CaO–21P_2O_5–19.7Al_2O_3–10.0CaF_2	• roughened Ti6Al4V	• Target size: 100 mm (square) • Target type: 1000 °C sintered compact disk of compressed MQ glass powder • Driving radio-frequency: *not mentioned* (probably, 13.56 MHz) • Target-to-substrate distance: *not mentioned* • Electrical powder: *not mentioned* • Sputtering gas: Ar • Sputtering pressure: 0.02 Pa ("1.5×10^{-4} *Torr*") → in fact, most-probably 0.2 Pa (1.5 mTorr) • Status: as-deposited	• Film thicknesses: *not given*; • Deposition rate: *not given*; • Deposition time: 120 min; • SEM showed coatings with flat, featureless surfaces; • The MG63 human osteoblast cell cultures tests indicated similar performances for the bare and glass-coated Ti6Al4V samples. The cells reached confluence after five days of culturing, and showed signs of mitosis;-Changes in the surface roughness had no effect on the osteoblast cell growth (SEM evidences only) ; • Possible deficient adherence/frailty of the coating at the edges of the samples was suggested.	[51]
45S5: 46.1SiO_2–26.9CaO–2.6P_2O_5–24.4Na_2O	• Ti6Al4V • Si • SiO_2 (quartz)	• Target diameter: 100 mm-Target type: mildly-pressed MQ powder at RT (grain size < 100 μm), NO sintering • Driving radio-frequency: 1.78 MHz • Target-to-substrate distance: 30 mm • Electrical powder: *not mentioned*-Sputtering gas: Ar & Ar + (7 &15 vol%) O_2 • Sputtering pressure: 0.23 – 0.7 Pa • Status: as-deposited & post-deposition heat-treated at 550 °C in air	• Film thicknesses: *not given*; • Deposition rate: *not given*; • Deposition time: 60 min; • Unusual rough surfaces were evidenced by SEM;-A high total sputtering pressure (0.7 Pa) and a high content of oxygen in the sputtering atmosphere (15 vol%) led an improved reproduction of the complex stoichiometry of the glass target.	[46]
	• Ti6Al4V • pure Ti • Corning® glass	• Target diameter: 110 mm-Target type: mildly-pressed MQ powder at RT (grain size < 7.5 μm), NO sintering • Driving radio-frequency: 1.78 MHz • Target-to-substrate distance: 30 mm	• Film thicknesses: ~ 420–1020 nm; • Deposition rate: ~ 7–17 nm/min (decreasing with the increase of sputtering pressure); • The bonding strength of **45S5** magnetron sputtered films was increased from ~ 29 to ~ 50 MPa by (*i*) the introduction of a co-sputtered compositionally graded	[84–86,88]

(*continued on next page*)

Table 1 (*continued*)

Cathode target SBG composition (mol%)	Substrate	RF-MS parameters	Main results	Refs.
		• Electrical powder: ~150 W • Sputtering gas: Ar • Sputtering pressure: 0.16; 0.3; 0.45 Pa • Status: as-deposited & post-deposition heat-treated at 650 and 700 °C/2h in air	buffer layer (*i.e.*, SBG_xTi_{1-x} (x = 0–1)), (*ii*) coupled with post-deposition annealing in air at moderate temperatures; • The as-deposited films readily dissolved in SBF, preventing the development of the sequential stages of the biomineralisation process; • The post-deposition annealing mitigated the rapid dissolution of the films in SBF, allowing for the formation of a well-developed apatite-like layer after 30 days of soaking; • The annealed **45S5**-derived films led to promising cytocompatibility responses when tested for 7 days in human primary osteoblast (hOB) cell cultures.	
	• Alumina	• Target diameter: *not mentioned*-Target type: mildly-pressed MQ powder at RT (grain size < 100 μm), NO sintering • Driving radio-frequency: *not mentioned* (probably, 13.56 MHz) • Target-to-substrate distance: *not mentioned* • Electrical powder: 200 W • Sputtering gas: Ar • Sputtering pressure: *not mentioned* • Status: as-deposited	• Film thicknesses: ~ 200 nm; • Deposition rate: ~ 3.3 nm/min; • The **45S5** sputtered films deposited onto alumina disks showed good mineralisation capacity (*i.e.*, formation of calcium phosphate ingrowths) when soaked in artificial saliva; • The RF-MS films enabled the recovery of the mechanical properties of the etched enamel by remineralisation processes upon soaking in artificial saliva at the homeostatic temperature.	[96,97]
58.5SiO_2–17.1CaO–4.5P_2O_5–7.9MgO–5.2Na_2O–6.8K_2O	• Ti6Al7Nb • Ti6Al4V • Corning® glass	• Target diameter: 110 mm • Target type: mildly-pressed MQ powder at RT, NO sintering • Driving radio-frequency: 1.78 MHz • Target-to-substrate distance: 30 mm • Electrical powder: *not mentioned* • Sputtering gas: Ar • Sputtering pressure: 0.16; 0.22 & 0.3 Pa • Status: as-deposited & post-deposition heat-treated at 550, 700, and 750 °C// 2h in air	• Film thicknesses: ~ 750–980 nm; • Deposition rate: ~ 12.5–16.3 nm/min (decreasing with the increase of sputtering pressure);-The highest used working gas pressure (*i.e.*, 0.3 Pa) enabled an improved target-to-substrate atomic substrate;-Noteworthy bonding strengths (pull-off) : >85 MPa (for the as-deposited and 550 °C-annealed samples) and of ~ 73 MPa (for the 750 °C-annealed samples) were evidenced; • The excellent adherence values were assigned to the pre-deposition argon ion plasma etching of the substrate (all samples, irrespective of crystalline state) and the inter-diffusion formation of a mix coating-substrate crystalline phase – $CaTiO_3$ (for the 750 °C-annealed samples); • Both amorphous (as-deposited and 550 °C-annealed) and crystallized (700 °C-annealed) films were bioinert, showing no signs of degradation and apatite-forming ability up to 30 days of testing in SBF.	[47,85]
58S: 59.8SiO_2–38.5CaO–1.7P_2O_5	• 3D macro-porous Ti6Al4V scaffolds	• Target diameter: *not mentioned* • Target type: sol–gel powder • Driving radio-frequency: *not mentioned* (probably, 13.56 MHz) • Target-to-substrate distance: 40–50 mm from the substrate centre (3-cathode confocal system tilted at 30°) • Electrical powder: 130 W • Sputtering gas: Ar • Sputtering pressure: 2.2 Pa • Status: as-deposited	• Film thickness: ~1 μm; • Deposition rate: ~ 4.2 nm/min; • SBG films were deposited onto 3D macro-porous metallic scaffolds; • The SBG coated scaffolds provided a favourable environment for human Saos2 cell proliferation and function: a two-fold increase in osteoblast cell proliferation with respect to the uncoated scaffold was noticed; • The application of SBG functional layers enhanced the deposition of extra-cellular matrix components such as decorin, fibronectin, osteocalcin, osteonectin, osteopontin, and collagen (type I and III); • The mineralisation of the extra-cellular matrix also experienced a two-fold increase.	[48]
1b: 39.9SiO_2–31.0CaO–2.6P_2O_5–13.3MgO–4.4Na_2O–4.4B_2O_3–4.4CaF_2	• pure Ti • Si • Corning® glass	• Target diameter: 110 mm • Target type: mildly-pressed MQ powder at RT, NO sintering • Driving radio-frequency: 1.78 MHz • Target-to-substrate distance: 30 mm • Electrical powder: *not mentioned*-Sputtering gas: Ar & Ar + (7 & 20 vol%) O_2 • Sputtering pressure: 0.2; 0.3 & 0.4 Pa • Status: as-deposited	• Film thicknesses: ~ 330–650 nm; • Deposition rate: ~ 4.7–9.3 nm/min (decreasing with the increase of sputtering pressure or with the increase of oxygen-in-argon dilution); • The **1b**-sputtered films presented very good adherence values in the range of ~ 45–73 MPa; • It was shown that it is possible to obtain a variety of film compositions from a single MQ target material by simply modifying the working pressure and oxygen dilution; • The **1b**-sputtered films elicited remarkable biomineralisation capacity, enabling the growth of thick crystalline CHA layers after 30 days of immersion in SBF.	[76,83,87,89]

(*continued on next page*)

Table 1 (*continued*)

Cathode target SBG composition (mol%)	Substrate	RF-MS parameters	Main results	Refs.
1d: 45.5SiO_2–30.3CaO–2.6P_2O_5–13.0MgO–4.3Na_2O–4.3CaF_2	• pure Ti • Si -Alpha-Bio® DFI dental Ti-based implants	• Target diameter: 110 mm • Target type: mildly-pressed MQ powder at RT, NO sintering • Driving radio-frequency: 1.78 MHz • Target-to-substrate distance: 25 mm • Electrical powder: 75 W-Sputtering gas: Ar & Ar + (10, 15 & 20 vol%) O_2 • Sputtering pressure: 0.2; 0.3 & 0.4 Pa • Status: as-deposited	• Film thicknesses: ~ 600 nm & 1 μm; • Deposition rate: ~ 4.6–8 nm/min (decreasing with the increase of sputtering pressure or with the increase of oxygen-in-argon dilution); • The best mechanical performances were obtained for the SBG films deposited at 0.4 Pa argon pressure: bonding strength (pull-off) of ~ 63 MPa, hardness of ~ 5.7 GPa, and elastic modulus of ~ 77 GPa; • The **1d**-derived SBG films presented excellent cytocompatibility in mouse fibroblast and human endothelial and dental pulp stem cell cultures; • The optimized deposition regime was successfully applied for the coating of real dental implants, which mechanically withstood the dynamic implantation stresses in cortical bone; • The implant coatings allowed for the preservation of their undifferentiated phenotype, with likely consequences on the prolongation of the implant's lifetime; • RF-MS was also conceptualized for the fabrication of resorbable sub-micrometre hollow cone-shaped formations (needles), which can find their use in the permeabilization of the blood–brain barrier (in the therapy of carcinoma and neurodegenerative disorders).	[55,77,78]
55.3SiO_2–20.5CaO–1.6P_2O_5–17.1MgO–5.5Na_2O	• Mg-0.8Ca alloy	• Target diameter: 110 mm • Target type: mildly-pressed MQ powder at RT, NO sintering • Driving radio-frequency: 1.78 MHz • Target-to-substrate distance: 35 mm • Electrical powder: 80 W • Sputtering gas: Ar • Sputtering pressure: 0.4 Pa • Status: as-deposited	• Film thickness: ~1 μm; • Deposition rate: ~ 5.5 nm/min; • Good target-to-substrate atomic transfer was obtained;-The SBG/Mg-0.8Ca samples had bonding strengths (pull-off) of ~ 30 MPa; • Good *in vitro* cytocompatibility was obtained when testing in human fibroblast (Hs27) and osteosarcoma (Saos-2) cell cultures; • SBG films reduced the weight loss and the hydrogen release rate of the Mg-based substrate, and improved its corrosion response in SBF and DMEM.	[79,82]
Z4S0: 38.5SiO_2–36.1CaO–5.6P_2O_5–15.2MgO–4.0ZnO–0.6CaF_2	• pure Ti • Si	• Target diameter: 110 mm • Target type: mildly-pressed MQ powder at RT, NO sintering • Driving radio-frequency: 1.78 MHz • Target-to-substrate distance: 35 mm • Electrical powder: *not mentioned* • Sputtering gas: Ar • Sputtering pressure: 0.4 Pa • Status: as-deposited	• Film thickness: ~1 μm; • Deposition rate: ~ 5.6 nm/min; • The composition and structure of the **Z4S0** SBG source material was well-replicated by using a long pre-sputtering time (60 min) and a sputtering argon pressure of 0.4 Pa;-It was also shown that the silica content of glasses (and thereby their network connectivity) can be intentionally and controllably increased by co-sputtering processes; • All films elicited biomineralization capacity, with the CHA development being slowed down by both network connectivity and increase of the biomimicry degree of the testing protocol (in terms of both medium composition and type of ambient);-All films elicited excellent cytocompatibility in mesenchymal stem cell cultures (highly similar to the biological control); • Proposals for the improvement of the apatite-forming ability testing protocols have been advanced.	[80]
FastOs®BG: 38.5SiO_2–36.1CaO–5.6P_2O_5–15.2MgO–4.0ZnO–0.6CaF_2 **&** **C2G3:** 38.5SiO_2–34.1CaO–5.6P_2O_5–16.2MgO–2.0CuO–3Ga_2O_3–0.6CaF_2	• pure Ti • Si	• Target diameter: 110 mm • Target type: mildly-pressed MQ powder at RT, NO sintering • Driving radio-frequency: 1.78 MHz • Target-to-substrate distance: 35 mm • Electrical powder: *not mentioned* • Sputtering gas: Ar • Sputtering pressure: 0.4 Pa • Status: as-deposited	• Film thickness: ~ 600 μm; • Deposition rate: ~ 5.6 nm/min;-Films with intentionally increased silica content (and thus, higher network connectivity) were deposited by co-sputtering processes from **FastOs®BG** and **C2G3** formulations, aiming for improved mechanical properties and moderate solubility; • Incorporation of Cu and Ga induced a slight polymerization of the films' SBG network compared to the undoped ones;-Cu and Ga doping experienced increased hardness (from ~ 5.8 to ~ 6.1 GPa) and critical load of scratch delamination (from ~ 4.3 to ~ 4.9 N); decreased elastic modulus (from ~ 136 to 127 GPa); and significantly improved wear resistance performance with respect to the undoped counterparts;-The bonding strength (pull-off) of both type of films was similar (~ 54 MPa); • The films yielded good cell proliferation in mouse fibroblast (NIH/3T3) cell cultures; • The Cu and Ga doped SBG films led to a prominent antibacterial activity against the *S. aureus* strain, reducing its growth by ~ 4 orders of magnitude with respect to control and the uncoated Ti substrate (at 24 h).	[81]

den Beucken *et al.* focused their researches on the *in vivo* testing of only HA and HA-SBG sputtered (post-deposition heat-treated) coatings [54,56,120]. The *in vivo* testing has been carried out on two animal models (*i.e.*, mandibles of Beagle dogs [54] & iliac crests of Dutch Saane milk goats [56,120]). Concerned about the poor adherence of their SBG films (due to technical limitations), no pure SBG control coating has been included in the *in vivo* assessments [54]. Conflicting *in vivo* biological findings were highlighted [54,56]. While the inclusion of S53P4 SBG into HA coatings did not enhance the biological *in vivo* performance when implanted in mandibles of Beagle dogs [54], it improved the early bone apposition when implanted in iliac crests of Dutch Saane milk goats [56], compared to the pure HA control. This could be assigned to different animal models, surgical procedures, local environment due to blood perfusion, and mechanical loading of the implant region. In the last article of the series [120], HA-SBG sputtered films were included into a comparative 12-week *in vivo* study (in goat model, having a certain variation in age and weight) together with pulsed laser (HA), electrospray (CHA), plasma-spray (HA with dissimilar crystallinities), biomimetically (HA & pure and Sr-doped octacalcium phosphate) and RF-MS deposited (HA and β-tricalcium phosphate) coatings. No precise information on the thickness of the coatings was given, being only categorized into two groups: (*i*) low thickness ("< 50 μm") in the case of the pulsed laser, electrospray and RF-MS deposited coatings; and (*ii*) high thickness (">50 μm") in the case of the plasma spray and biomimetically deposited ones. The conclusion of their study was that plasma-sprayed HA-based coatings had a superior osteophilic effect with respect to the other coatings deposited by different techniques [120].

The second type of sputtered composite coatings was developed by the research team led by M. Ferraris and included films of tuneable thickness (from few nanometres to half a micrometre) in which silver nanoclusters were embedded in a matrix of pure silica glass (silver and silica co-targets were used during the sputtering process) [123]. These coatings, which are non-bioactive in the sense that they do not promote apatite formation, were initially developed to provide a wide range of substrate materials for everyday life (polymers, metals, glasses, textiles) with antibacterial properties [124]. Potential application as antibacterial coating on the surface of polymeric ocular prostheses was reported using *S. aureus* as bacterial strain [125]. A virucidal effect against coronavirus SARS-CoV-2 was also demonstrated in 2020 [126]. However, the silica glass matrix underwent resorption in biological fluids over time, which limits the duration of the antibacterial/antiviral treatment; therefore, the search for more chemically stable matrixes seems to be advisable.

3.3. Standalone phosphate-based bioactive BG coatings

Unlike SBGs, which are intended to form a permanent bone-like apatite layer, PBG counterparts may fully resorb by hydrolysis of the P–O–P backbone, allowing their cationic constituents to leach and to act as temporary nutrients at the implant site [50]. Their range of dissolution profiles can be tailored from several years in extreme environments, as shown by phosphate glasses used in the nuclear waste industry, to several minutes depending on the strength of ionic cross-linking and on the degree of network connectivity [90,127–129]. The research area covering MQ PBGs and their tailorable properties has been tackled in numerous studies, aiming at an assortment of applications, ranging from stem cells carrying microspheres, fibres for reinforcing resorbable polymer matrices, fracture fixation devices to osteogenic scaffolds [130–135]. Their application as thin-films intended for the rapid release of osteogenic and antimicrobial ions at implant surfaces is limited to the studies published by Stuart *et al.* [50,90–95], which debuted in 2015 [50]. Their *in vitro* cytocompatibility and antibacterial properties have recently showed promise for future *in vivo* trials [94,95].

In contrast to the bulk of work performed on SBG films [47,49,55,76–85,87–89], which employed ~ 110 mm diameter powder targets pressed at room-temperature; target-substrate distances of 30–55 mm; and 1.78 MHz RF power sources, the PBG film research conducted at University of Nottingham by Stuart *et al.* [50,90–93,95] made use of ~ 57 and ~ 75 mm large disk shaped MQ pre-formed targets of glass formulation of up to five network modifying oxides; target-substrate distances of 40–60 mm; and the conventional (commercial) RF frequency of 13.56 MHz. Deposition from such targets achieved consistent deposition stoichiometries over thousands of hours of sputtering from a single target, when operated at very low power densities of ~ 1.3 W/cm^2 to prevent thermally induced phase change of the target [50,90]. As a result, low deposition rates of less than ~ 2.6 nm min^{-1}

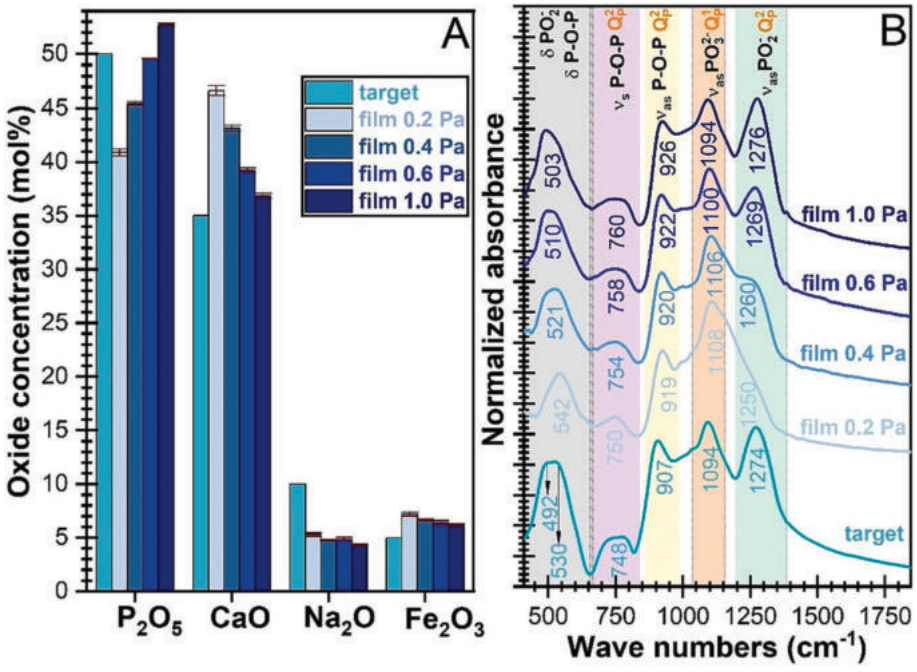

Fig. 9. (A) Compositional variation of the oxide concentrations of PBG films with the increase of the working pressure, with respect to the concentration of the source material. (B) Comparative FTIR spectra of the PBG films deposited at different sputtering pressures. Reproduced with permission from Ref. [94].

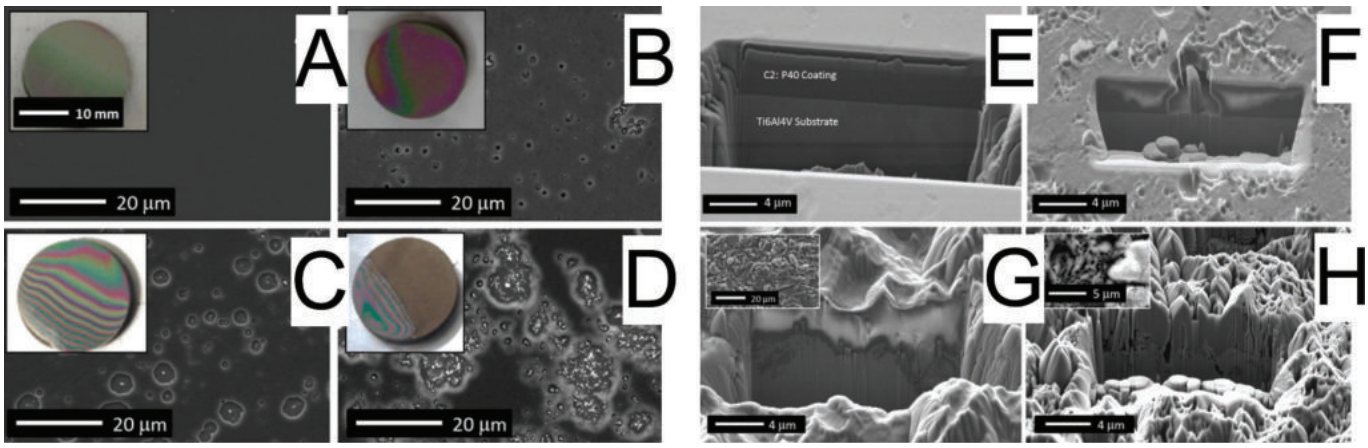

Fig. 10. Complete coating degradation of PBG on polished Ti6Al4V substrates in distilled water representing: (A) coated and subsequent degradation for (B) 4 h, (C) 16 h (D) 24 h. Cross-sectional FIB-SEM of an as-deposited coating on polished Ti6Al4V. (B) Micrograph of a 16 h degraded coating, milled into a corrosion pit. (C and D) on sandblasted Ti6Al4V. Reproduced with permission from Ref. [90].

were constantly reported throughout the studies [50,90–93,95,136]. Films from a few tens of nanometres up to ~ 25 µm were prepared [91,95]. However, in a joint publication Stuart & Stan *et al.* [94] accurately replicated the recipe applied for the SBG films deposition at NIMP (*i.e.*, powdered targets, target-substrate distance of 35 mm, 1.78 MHz RF generator, powder density of ~ 1.05 W/cm^2). Such experimental conditions enabled an increase of the deposition rate to ~ 3.9–4.7 nm min^{-1} (depending on the working gas pressure). Normally, an increase of the driving frequency will result in prolonging of the time spent by electrons in the electric field, and thus to an augmented electron energy, and subsequently elevated electron temperature and plasma potential, but then also to a diminution of the electron density and ion flux, which can only be recovered by applying higher sputtering powers to the cathode [71,137]. The higher deposition rates recorded when using a lower driving frequency (*i.e.*, 1.78 MHz), are in line with Yang *et al.* studies [138] on Ag films, which showed a higher deposition rate for 2 MHz *vs.* 13.56 MHz. This was facilitated by the higher maximal energy and flux density of ions found at 2 MHz (56.27 eV and 0.0559 A m^{-2}) with respect to 13.56 MHz (44.07 eV and 0.0313 A m^{-2}) [138]. Nevertheless, the increase of deposition rates (and thus, productivity) remains a future challenge for the industrialization of BG films for healthcare applications. Larger-sized cathode targets will aid both higher applied power densities (and higher deposition rates) and an excellent film uniformity over the surface of large-sized biomedical fixtures.

Regardless of the deposition system/configuration, both as-deposited and post-deposition annealed PBG thin-films consistently achieved high mechanical pull-off adhesion in excess of 70 MPa on commercially pure Ti or Ti6Al4V substrates, which are higher than those recommended by the FDA regulations [14] for calcium-phosphate coatings (*i.e.*, 50.8 MPa pull-off) on implant surfaces, paving the way

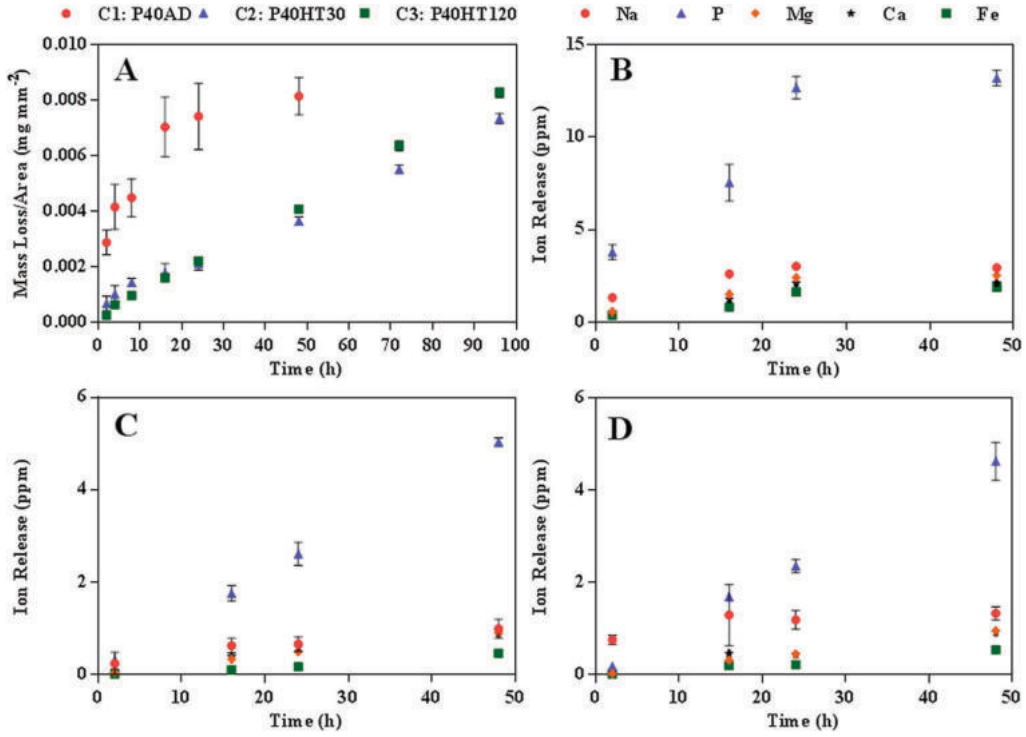

Fig. 11. Degradation of C1: P40AD, C2: P40HT30 and C3: P40HT120 the PBG coatings. (A) Dissolution rates up to 96 h in distilled water and ion release profiles following dissolution in ultra-pure water up to 48 h (B) C1: P40AD (C) C2: P40HT30 and (D) C3: P40HT120. Reproduced with permission from Ref. [92].

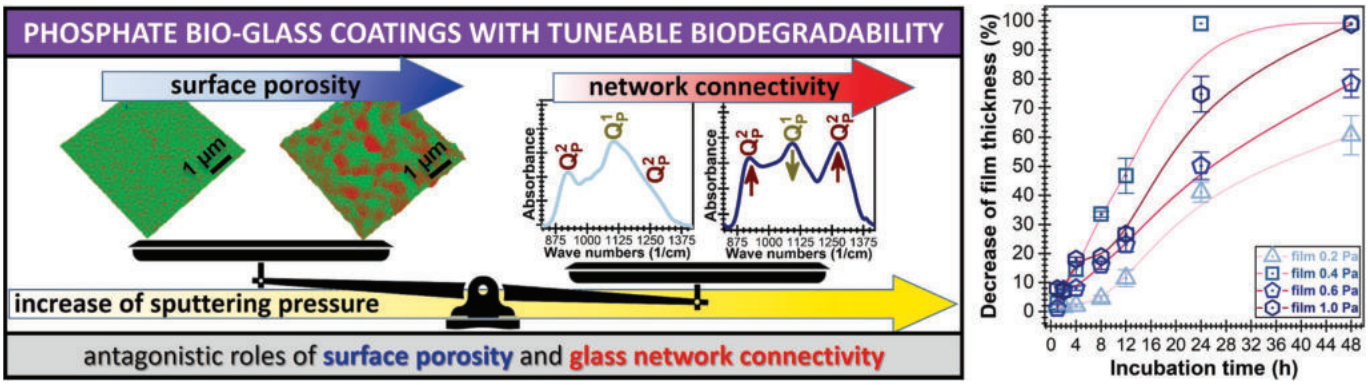

Fig. 12. The antagonistic roles of surface porosity and network connectivity, conditioned by the sputtering argon pressure, on the biodegradability of PBG films. Reproduced with permission from Ref. [94].

for further utilization and functional optimization [92].

The composition and structure of the PBG sputtered layers were intricately controlled by manipulating the "preferential sputtering" effect [50,91]. It was showed that adjustment for non-stoichiometry target-to-film changes by over or under compensating for particular oxides in the MQ pre-form was a consistent method for tailoring the thin-film physical–chemical properties [50,91]. A detailed investigation of P_2O_5, MgO, CaO, Na_2O and Fe_2O_3 containing MQ PBGs suggested preferential sputtering in the order P < Fe < Ca < Mg < Na, which correlated to the relative dissociation energies of each network modifier bound to oxygen of (~818 or 1227, 928, 788, and 257 kJ mol^{-1} for Fe, Ca, Mg, and Na, respectively). Phosphorous, the network former, being heavily shielded by the abundant network modifiers, experienced a considerable stoichiometric loss in the thin-films [50]. The working gas pressure was found as a key variable to tailor the glass composition and structure (*i.e.*, network connectivity). Superior replication of the source (cathode target) glass oxide concentration (including P_2O_5) (Fig. 9A) and structural features (Fig. 9B) was achieved when using higher argon pressures (*i.e.*, 0.6 and 1.0 Pa) and a low target-to-substrate distance (*i.e.*, 35 mm) [94].

The discovered structural intricacies were highly-relevant and explicative for the observed dissolution profiles of PBG thin-films, where a dual, non-linear rapid dissolution profile was observed when submerged in deionized water. Iron-containing PBG compositions of $28P_2O_5$–$27MgO$–$20CaO$–$19Na_2O$–$6Fe_2O_3$ and $40P_2O_5$–$24MgO$–$16CaO$–$16Na_2O$–$4Fe_2O_3$ (mol%) were deposited to several microns with the intention of tailoring dissolution rate to several weeks. Instead, it was found that both highly-polymerized PBG thin-film surfaces were superhydrophilic, exhibiting droplet contact angles of < 1°. The PBG films dissolved rapidly, showing a $t^{1/2}$ profile, where 20% of the 2.7 μm thick film dissociated within the first 2 h of immersion. The remainder of the film (~2.1 μm) dissolved linearly over the following 20 h, showing dissolution rates of at least two times slower than the compositionally equivalent MQ glasses [90]. The $28P_2O_5$–$27MgO$–$20CaO$–$19Na_2O$–$6Fe_2O_3$ and $40P_2O_5$–$24MgO$–$16CaO$–$16Na_2O$–$4Fe_2O_3$ (mol%) films degraded (within the linear regimes) at rates of 50×10^6 and 210×10^6 mg $mm^{-2}h^{-1}$, respectively. In phosphate buffered saline, the dissolution similarly began at a rapid rate and plateaued within hours, forming stable and film protecting precipitates to suggest that certain compositions or conditions of PBG films could both accelerate biomineralisation towards osseointegration and deliver therapeutic species with osteogenic influence. The formed precipitate remained stable over the following 21 days of experimentation period. Surface imaging of degrading PBG films showed in-homogenous dissolution and dispersed corrosion-like pitting (see Fig. 10).

Several attempts were made by Stuart *et al.* to optimize the composition of PBG thin-films to achieve extended dissolution regimes [50,90–92]; however, due to the observed highly polymerized structural properties, this was not achieved within the tested processing window (conventional RF of 13.56 MHz) or glass composition. Contrarily to SBG systems, where a higher content of network formers (*i.e.*, silicate units) results in a less-soluble highly-polymerised structure (possessing high network connectivity), a higher-polymerisation of PBG structures results in a higher hydration ability and susceptibility to hydrolysis. Thereby, a high P_2O_5 content leads to faster degradation of the PBG, whilst in the case of the lower P_2O_5 content glasses (with a more depolymerised glass network), the improved dissolution durability/stability is given by the network crossing-linking *via* network modifying ions. However, the nature of the network modifying ions and their cross-linking ability are key factors. For instance, multivalent ions (such as iron) could create

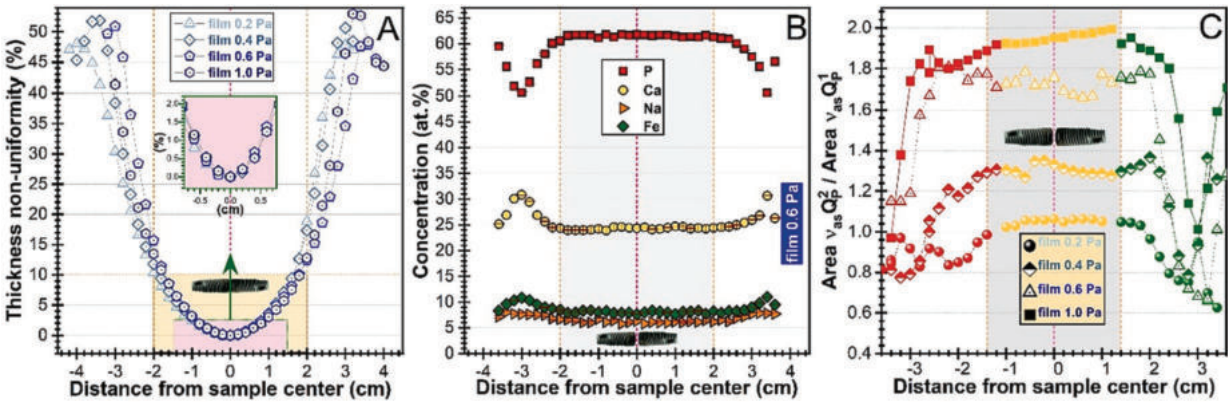

Fig. 13. Cross-area uniformity variation with sputtering pressure in terms of (A) thickness, (B) composition and (C) structure of PBG films deposited by 1.78 MHz RF-MS. Reproduced with permission from Ref. [94].

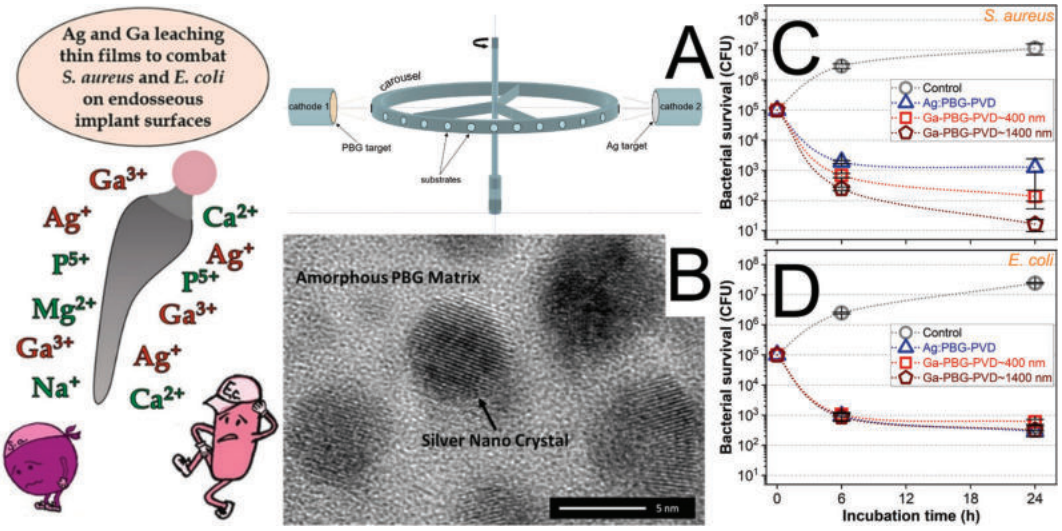

Fig. 14. (A) Illustration of the "dual target consecutive co-sputtering" process; (B) HR-TEM image showing the microstructure of the Ag-PBG composite thin-film. (C, D) Time evolution of the antibacterial activity of the (~ 46 nm) Ag-PBG composite and the (~ 0.4 and ~ 1.4 μm) Ga-doped PBG implant-type coatings against (C) *S. aureus* and (D) *E. coli* strains. The data are represented as logarithmic values of CFU mL^{-1} of bacterial cells. Reproduced with permission from Ref. [95].

very durable PBG structures, whilst monovalent ions (such as Na) break the chains and consequently lead to higher dissolution rates. As a result, a compositional/structural trade-off design is always needed for achieving PBGs with predictable biological performance.

Yet, elongated dissolution profiles of up to 120 min were achieved for $40P_2O_5$–24MgO–16CaO–$16Na_2O$–$4Fe_2O_3$ (mol%) 2.7 μm-thick films by post-deposition annealing and crystallization at 500 °C in argon to form a glass–ceramic containing Fe_2O_3 hematite phase. This successfully eliminated the rapid surface dissolution previously observed up to 2 h and also enabled a controlled linear ionic release of all ionic constituents within 4 days (2.4–3 times slower for the annealed coatings), as assessed by inductively coupled plasma mass spectroscopy (ICP-MS) (Fig. 11) [92].

Important strides in reducing the degradation of PBG films were made in 2021 [94] by employing a $50P_2O_5$–35CaO–$10Na_2O$–$5Fe_2O_3$ (mol%) formulation and a sputtering regime with a single notable difference, the RF frequency of 1.78 MHz (since the other variables – target-to-substrate distance, gas pressure, power density – were largely similar). The degradation of the PBG sputtered films was found to be conditioned by two antagonistic factors of influence: (*i*) the network connectivity of the phosphate glass and (*ii*) the degree of films surface porosity (Fig. 12). An increased P_2O_5 content of the PBG films and moderate-sized pits/pores (ubiquitously found for sputtered PBG films [91,94]) led to an extended degradation in cell culture medium (DMEM-10%FBS) to> 48 h. First cytocompatibility tests (human fibroblast cell line, Hs27) performed on PBG sputtered films were reported within the same study, with highly promising results. Moreover, Tite, Stuart & Stan *et al.* [94] showed that cross-area uniformity (structurally and compositionally) over 30 mm was achievable for PBG films using a laboratory-grade RF-MS set-up, having beneficial implications for the future scale up application in dental implants in particular (Fig. 13).

Both Ga and Ag were included in the PBG network ($40P_2O_5$–15CaO–$16Na_2O$–24MgO–$5Ga_2O_3$ (mol%)) and tested against *S. aureus* and *Escherichia coli* bacterial strains [66]. The benefit of rapid dissolution in the early stages of implantation and shedding of the entirety of the film within 24 h was leveraged to assess feasibility of incorporating Ga ions into a 1.4 μm-thick PBG film structure as an emerging and potentially pungent antibacterial agent [93,95]. Ga is known to disrupt the metabolic functions of bacteria by "disguising" itself as Fe^{3+}. The cell mistakenly uptakes Ga^{3+} and is unable to perform the redox cycling to reduce to Ga^{2+}, thereby, starving the bacteria. To similar effect, the well-known efficacy of Ag nanoparticles (NPs) was incorporated by a new technique termed "dual target consecutive co-sputtering" (Fig. 14). This methodology was successfully trialled to incorporate Ag NPs of ~ 5 nm in diameter throughout a PBG film matrix. This was achieved by employing RF-MS deposition from two independent cathode targets (50.8 mm in diameter) – Ag and MQ PBG ($57P_2O_5$–12CaO–14MgO–$14Na_2O$–$3Fe_2O_3$ (mol%)) – and applying different target powers of 5 and 100 W, respectively. The thickness of the Ag-PBG film was confirmed through high-resolution transmission electron microscopy (HR-TEM). Chemical analysis using EDXS confirmed the concentration of Ga_2O_3 in the final coating showing a 15 at.% increase with respect to the target composition. Ag-PBG films were limited to 46 nm thick. However, the presence of metallic silver inhibited the dissolution rate of the film, whilst facilitating early antibacterial efficacy. At the 24 h timepoint, the 1.4 μm Ga containing PBG films and 46 nm Ag-PBG films showed 6-log and 4-log reductions in gram-positive *S. aureus* colony forming units (CFU's), respectively, and a 5-log reduction for both coatings against *E. coli*. All coatings were shown to be cytocompatible with respect to human fibroblast (Hs27) and mesenchymal stem (hMSC) cells, demonstrating great potential for preventing post-operative implant infection and supported the next step of advanced *in vitro* assays and development towards *in vivo* testing.

In a separate study, Sato *et al.* [98] deposited films by RF-MS using an inverted phosphate containing glass target (*i.e.*, 65ZnO–$30P_2O_5$–$5Nb_2O_5$ (mol%)), made by pelleting powder at a pressure of ~ 50 MPa. Structurally, the deposited films largely consisted of pyrophosphate (Q_P^1) and orthophosphate (Q_P^0) groups, with only trace amounts of metaphosphate (Q_P^2) units. The source target material did not contain metaphosphate (Q_P^2) units, whilst it elicited a lower pyrophosphate (Q_P^1)/orthophosphate (Q_P^0) groups ratio with respect to the RF-MS films, as evidenced by ^{31}P magic angle spinning nuclear magnetic resonance (MAS-NMR). From biological standpoint, the films showed durability when immersed in Tris buffer solution (*i.e.*, degradation rate of ~ 10 nm/day), cell viability and metabolic activity similar to the bare silica-glass substrates (when tested in human-derived osteosarcoma cell (Saos-2) cultures), and excellent antibacterial effects against *S. aureus* and *E. coli*.

The compositions of PBG targets, the types of substrates, the RF-MS parameters and the main outputs of the performed studies are summarized in Table 2.

4. Magnetron sputtered glass films: New insights into their structural origin

Pioneering research that definitively answer a longstanding question

Table 2
The main results of depositing various PBGs by RF-MS onto different substrates.

Cathode target SBG composition (mol%)	Substrate	RF-MS parameters	Main results	Refs.
T1: $40P_2O_5$–16CaO–24MgO–$20Na_2O$ **T2:** $45P_2O_5$–16CaO–24MgO–$15Na_2O$ **T3:** $50P_2O_5$–16CaO–24MgO–$10Na_2O$ **T4:** $50P_2O_5$–14CaO–22MgO–$12Na_2O$–$2Fe_2O_3$ **T5:** $50P_2O_5$–14CaO–20MgO–$12Na_2O$–$4Fe_2O_3$ **T6:** $51.5P_2O_5$–14CaO–18.5MgO–$11Na_2O$–$5Fe_2O_3$	• pure Ti disks • borosilicate glass cover slides	• Target diameter: 75 mm • Target type: Pre-formed disks fabricated by melt-quenching • Driving radio-frequency: 13.56 MHz • Target-to-substrate distance: 60 mm • Electrical powder: 20–140 W • Sputtering gas: Ar • Sputtering pressure: 0.28–1.87 Pa • Status: as-deposited	• First instance of PBG film deposition by RF-MS; • Film thicknesses: ~1.8–2.4 μm; • Deposition rate: ~1.6–1.9 nm/min; • The sputtering yields for the elements within the quaternary (T1–T3) and quinternary (T4–T6) oxides PBGs were dependent of the chemical bonding and momentum exchange interactions at the surface and subsurface of the cathode target; • The increase of the sputtering pressure from 0.28 to 1.87 Pa led to improved target-to-substrate atomic transfer; • Crystallisation events in the target surface were observed at power > 100 W, as effect of plasma bombardment heating.	[50]
T6: $51.5P_2O_5$–14CaO–18.5MgO–$11Na_2O$–$5Fe_2O_3$	• Ti6Al4V (grade 5) polished and sandblasted disks • borosilicate glass cover slides	-Target diameter: 75 mm • Target type: Pre-formed disk by melt-quenching • Driving radio-frequency: 13.56 MHz • Target-to-substrate distance: 40 mm • Electrical powder: 60 W • Sputtering gas: Ar • Sputtering pressure: 0.28 & 1.33 Pa • Status: as-deposited & post-deposition heat-treated at 500 °C/30 min and 500 °C/120 min in argon	• Film thicknesses: ~1.7 & ~2.7 μm; • Deposition rate: ~1.45–2.3 nm/min; • Surface XPS analyses showed structural differences between the PBG sputtered films and the source MQ target glasses: The PBG sputtered films had a higher bridging oxygen/non-bridging oxygen bonds ratio (*i.e.*, 34.2/65.8 (%) *vs.* 20.5/79.5 (%), generating metaphosphate $(PO_3)^-$ (Q_P^2) *vs.* less soluble pyrophosphate $(P_2O_7)^{4-}$ (Q_P^1) and orthophosphate $(PO_4)^{3-}$ (Q_P^0), with respect to the cathode target; • As-deposited and heat-treated PBG coatings exhibited pull-off tensile adhesion values > 74 MPa, surpassing the ISO (*i.e.*, 15 MPa) and FDA (*i.e.*, 50.8 MPa) requirements for HA implant coatings;-The heat-treated coatings deposited onto sandblasted substrate yielded superior adhesion (assessed by scratch-testing) , interfacial failure occurring at critical loads of 8.6–11.3 N, with respect to the ones deposited on mirror-polished substrates (2.3–5.0 N); • The highly soluble PBG coatings experienced in the first 2 h a $t^{1/2}$ degradation dependence in distilled water, followed by a more characteristic linear profile owned to subsequent less soluble layers; • The coatings immersed in degraded in phosphate-buffered saline precipitated a stable amorphous layer within 24 h; • The heat-treatments mitigated the exponential degradation rate met for the as-deposited coating in the first 2 h, and enabled linear degradation rates (reduced by factor of 2.4–3) within a 24 h window for the partially crystallized PBG coatings.	[90,92]
$48P_2O_5$–16CaO–24MgO–$12Na_2O$	• Ti6Al4V (grade 5) polished and sandblasted disks • borosilicate glass cover slides	• Target diameter: 75 mm • Target type: Pre-formed disk by melt-quenching • Driving radio-frequency: 13.56 MHz • Target-to-substrate distance: 40 mm • Electrical powder: 60–80 W • Sputtering gas: Ar • Sputtering pressure: 1.33 & 1.6 Pa • Status: as-deposited	• Film thicknesses: ~14–25 μm; • Deposition rate: ~1.45–2.6 nm/min; • Short-range structural difference between PBG deposited films and MQ source materials were highlight by 31P MAS-NMR, XPS and FTIR spectroscopy and DTA investigations; • The PBG magnetron sputtered films were highly polymerised with respect to the MQ materials of identical compositions, which is attributed to the etching of the coatings during deposition owned to ion bombardment; • The T_g points of the PBG sputtered coatings were with 13.7–20.1 °C lower than their MQ equivalent glass counterparts; • The RF-MS PBG layers are more durable than the equivalent MQ glasses.	[91]
$65ZnO–30P_2O_5–5Nb_2O_5$ (**inverted glass**)	Pure silica-glass	• Target diameter: 50 mm • Target type: powder pelleted under a pressure of ~ 50 MPa • Driving radio-frequency: *not mentioned* (probably 13.56 MHz) • Target-to-substrate distance: *not mentioned*. • Electrical powder: 50 W • Sputtering gas: Ar • Sputtering pressure: 5.0 Pa • Status: as-deposited	• Film thickness: ~ 170 nm; • Deposition rate: ~ 0.6 nm/min; • Structural differences with respect to the source material were noted; –No cytotoxic effects were noticed. The films recorded similar human-derived osteosarcoma cell (Saos-2) viability and metabolic activity with respect to the bare, silica-glass, substrates;-Films exhibited relatively high durability in a Tris buffer solution (~10 nm/day), and showed extremely slow ion-release; • Antibacterial effects against *S. aureus* and *E. coli* were recorded.	[98]

(*continued on next page*)

Table 2 (*continued*)

Cathode target SBG composition (mol%)	Substrate	RF-MS parameters	Main results	Refs.
$50P_2O_5$–35CaO–$10Na_2O$–$5Fe_2O_3$	Si	• Target diameter: 110 mm • Target type: powder mildly-pressed in a metallic dish • Driving radio-frequency: 1.78 MHz • Target-to-substrate distance: 35 mm • Electrical powder: ~100 W • Sputtering gas: Ar • Sputtering pressure: 0.2–1.0 Pa • Status: as-deposited	• Film thicknesses: ~ 700–850 nm; • Deposition rate: ~ 3.9–4.7 nm/min; • The possibility to fine tune the composition, structure and morphology, and thus, the biological interaction of the PBG films by conveniently modifying the sputtering pressure was revealed; • The complex stoichiometry and structure of the source PBG material is well-replicated when using sputtering argon pressures of 0.6 and 1.0 Pa; • The antagonistic roles of the network connectivity and surface porosity of the PBG films on their degradation behaviour in cell culture medium were evidenced;-Degradation in cell culture medium (DMEM-10%FBS) was extended beyond 48 h; • A cross-area uniformity over a diameter of ~ 30–40 mm was indicated, constituting an important technological step for their future scale-up and biomedical application; • The PBG films yielded Hs27 fibroblast cell proliferation responses comparable to the biological control.	[94]
$57P_2O_5$–12CaO–14MgO–$14Na_2O$–$3Fe_2O_3$	Pure Ti	• Target diameter: 57 mm • Target type: Pre-formed disk by melt-quenching • Driving radio-frequency: 13.56 MHz • Target-to-substrate distance: 40 mm • Electrical powder: 100 W (on PBG target) and 5 W (on Ag target) • Sputtering gas: Ar • Sputtering pressure: 0.36 Pa • Status: as-deposited	• Film thickness: ~ 46 nm;-Ag nanoparticles (5 nm in diameter) were embedded into the PBG film by employing a new deposition concept denominated "dual target consecutive magnetron co-sputtering"; –No cytotoxic effects were signalled for the Ag-PBG composite coatings (against Hs27 fibroblast and mesenchymal stem cell lines), only a marginal cell proliferation inertia; • Ag ion released could only by quantified in the case of degradation tests in nutrient broth, with a concentration value of 9 ppm being revealed after 24 h of immersion; • After 24 h, marked antibacterial efficacies against *S. aureus* and *E. coli* bacterial strains of 4-log and 5-log CFU reduction, respectively, were recorded.	[95]
$51.5P_2O_5$–14CaO–18.5MgO–$10Na_2O$–$6Ga_2O_3$	Pure Ti	• Target diameter: 75 mm • Target type: Pre-formed disk by melt-quenching • Driving radio-frequency: 13.56 MHz • Target-to-substrate distance: 40 mm • Electrical powder: 60 W • Sputtering gas: Ar • Sputtering pressure: 1.33 Pa • Status: as-deposited	• Film thicknesses: ~ 400 nm–1.45 μm; • Deposition rate: ~ 1.21 nm/min; • The hardness and elastic modulus values of the Ga-doped PBG film were of 4.7 and 69.7 GPa, respectively, thus, similar to the plasma sprayed HA and dental enamel, and higher with respect to femoral cortical bone;-The sputtered PBG appeared to be denser (3.5 *vs.* 2.7 g cm^{-3}) and more polymerised than the compositionally equivalent MQ glasses; • The Ga:PBG coatings exhibited high surface energy of ~ 75 mN/m, determined by the hydrolytic nature of the P–O–P structural bonds; • Ga was released from the ~ 1.45 μm coating after 24 h of immersion in deionized water, nutrient broth, and cell culture medium (DMEM) at concentrations of ~ 6, 27, and 4 ppm, respectively, unveiling dissimilar degradation profiles;-The films presented excellent cytocompatibility with human Hs27 fibroblast and mesenchymal stem cell (hMSC) cultures; • The Ga:PBG films exhibited excellent antibacterial effects against both *S. aureus* (6-log CFU reduction for Ga:PBG-PVD≈1400 nm & 5-log CFU reduction for Ga-PBG-PVD≈400 nm) and *E. coli* (5-log reduction for both coatings) with respect to the bare pure Ti substrate.	[93,95]

[139] of whether the physical vapour inorganic glass-derived deposits are structurally analogous to conventional MQ glasses was performed by Stan, Stuart & Ferreira [76–78,80,81,89,91,93–95]. The cross-sectional transmission (SBG case) and scanning (PBG case) electron microscopy analyses disclosed that the top-to-bottom growth morphology of the both type of sputtered films was smooth, compact and featureless, archetypal for glass materials [77,95]. Beyond showing the amorphous status (long-range disorder) of the SBG and PBG films by grazing incidence X-ray diffraction [76,93,94], importantly, information on the short-range ordering and comparative structural architecture of the MQ and RF-MS deposited glasses was successfully inferred by Fourier transform infrared (FTIR) spectroscopy (in both attenuated total reflectance and transmission modes, when employing titanium and silicon substrates, respectively), Raman spectroscopy and X-ray photoelectron spectroscopy (XPS), in both SBG [76–78,80,81,89] and PBG [91,93–95] cases. When the composition of the source (cathode target) materials was well-replicated into BG films, the FTIR spectroscopy analyses unveiled analogous (in terms of both amplitude and wave number position) broad IR absorption bands for both the MQ fabricated and RF-MS deposited glasses [80,81,94] (Fig. 7A & 9B), indicating that the magnetron sputtering derived structures are genuine glass materials, and not immiscible mixes of amorphous oxides. Moreover, modifications in the network formers/network modifiers ratios of the films relative to the MQ parent material (induced by changes in the RF-MS parameters), translate into the same regular network connectivity effects as for MQ glasses, *i.e.*, mirrored evolution of IR spectral components generated by specific populations of silicate and phosphate structural units with different numbers of bridging oxygen (BO) atoms [77,80,81,89,94]. Markedly, the fingerprint region of the FTIR spectra of SBGs is dominated by three distinct bands appertaining to the asymmetric stretching vibrations of (*i*) the Si–O–Si bonds in all the silicate tetrahedrons (transverse- and longitudinal-optical modes) (~1200–1000 cm^{-1}) and (*ii*) Si–O bonds in $Q^3_{Si} + Q^2_{Si}$ (with one and two non-bridging oxygen atoms (NBOs), respectively) and in $Q^1_{Si} + Q^0_{Si}$ (with three and four NBOs, respectively) (~1000–800 cm^{-1}) units [81]. Similarly to SBGs, the FTIR spectra of PBG films were found to elicit all the IR absorption bands observed for the MQ counterparts [93,94]. The IR absorption envelopes of the MQ and RF-MS PBGs are dominated by the asymmetric stretching of the (*i*) P–NBO bonds in $(PO_2)^-$ intermediate Q^2_P units (~1300–1200 cm^{-1}) and $(PO_3)^{2-}$ terminal Q^1_P units (~1150–1050 cm^{-1}) and (*ii*) P–O–P links in Q^2_P structural units (~950–900 cm^{-1}) [93,94]. The Raman spectroscopy analyses, performed so far only for the PBG sputtered films, fully supported the FTIR spectroscopy findings [93]. XPS was another powerful analysis tool employed. Its sensitivity permitted to delve the local structural order or chemical bonding configuration of the RF-MS BG films, as well as to disclose the chemical state of therapeutic cation dopants [77,81,89,91,95]. For instance, the O 1s core electron level region can be used to determine the shares of the BO and NBO bonds: *i.e.*, Si–O–Si (higher energy component positioned at a binding energy of ~ 532 eV) and Si–NBO (lower energy component centred at ~ 530 eV) for SBGs [77,81,89], and P–O–P (higher energy component positioned at ~ 533–534 eV) and P–NBO (lower energy component centred at ~ 531–532 eV) for PBGs [93,95]. Highly-eloquent studies, alleviating any possible doubts, were performed by Stuart *et al.* through ^{31}P MAS-NMR spectroscopy [91,93] and differential thermal analysis (DTA) [91] on PBG films deposited by RF-MS. ^{31}P MAS-NMR spectroscopy was used for the first time on thin film inorganic glass films to ascertain the proportion of Q^n_P species within the structure (a direct measure of network connectivity) of MQ and RF-MS counterparts. ^{31}P MAS-NMR spectroscopy results obtained by comparing three compositionally equivalent RF-MS films and MQ glasses indicated that the coatings elicited an increased network connectivity, with the concentration of Q^2_P species being higher (*i.e.*, 23% to 45%) compared to the MQ glass complements (*i.e.*, 9% to 32%). Convincingly, the DTA analyses, also carried out for the first time on RF-MS deposited inorganic glasses (regardless, if silica- or phosphate-based), demonstrated that the RF-MS film materials are exhibiting definite T_g points (Fig. 15), albeit showing shallow endotherms, a characteristic expected from highly-aged glasses. This is a somewhat expected phenomenon, similar to what has been found by researchers in the field of polymeric and organic vapour deposited glasses with respect to super-cooled counterparts [140–142]. Most recently, the glassy nature of the SBG sputtered films was confirmed by X-ray absorption near edge structure (XANES) measurements (work in progress). XANES informed that the short-range ordering and the chemical state of the elements in RF-MS films was equivalent to that found in the MQ bulk glass.

5. Overcoming challenges

Making strides in the field of medical coatings has become vital for improving the performance of a variety of medical devices (endosseous implants included) with the aim of extended lifetimes from 15 years, in the case of bioinert implants, to achieving 50 + years with bioactive implants. Bioactive and ion releasing coatings could greatly enhance biocompatibility, osseointegration, corrosion resistance, and further provide marked anti-microbial alternate defences. In spite of their remarkable biological performance, bioactive glasses are still late to make the jump to real-life implant coating applications in the clinical practice. The development of the BG implant coatings and their clinical use was hindered for several decades by their poor bonding strength to the metallic substrates and overall deficient performance under dynamical biomechanical stresses. Catastrophic failure of the coating-implant interface would likely require revision/substitution emergency surgeries. However, the most recent generational developments in SBG compositional systems have yielded both lower CTEs (even matching those of Ti and its medical alloys) and unaltered or even augmented (by designed metallic oxide substitutions) biological properties. This has re-accelerated interest in reliable SBG-based implant coatings, and thus led to worldwide resurgence.

In the period 2003 – to date research was devoted to the promotion of RF-MS as a highly compelling deposition technology to pursue and contribute to the long-trailing desiderate of BG implant coatings. Besides, the well-known capacity of this deposition technology to be translated to industry, its noteworthy versatility and flexibility allowed for the implementation of protocols which overcame – for the most part – a series of development barriers, *i.e.*, bonding strength, replication of the composition and structure of the source (target) materials, "line-of-sight" deposition (poor step coverage), low deposition rate, or economical manufacturing.

Largely, the adherence of the BG films deposited RF-MS is no longer an issue, being in excess of the minimal value endorsed by the ISO 13779–2:2018 (*i.e.*, 15 MPa) [44,49,88] even for the high-CTE BG systems, and being commonly close or higher than the FDA 1997 recommendation (*i.e.*, 50.8 MPa) [77,81,89,92,93] for the low-CTE BG systems. Solutions for the increase of bonding strength for the most demanding BG were successfully implemented relying on the insertion of thin-layers with graded BG-Ti composition [88] and atomic inter-diffusion by post-deposition annealing treatments [47,49].

RF-MS was criticized early on for being unable to accurately reproduce the composition of complex materials, such as BGs, because lighter species are more easily expelled off the target surface. The systematic studies carried out over the last years showed that this can no longer be considered the Sisyphus mountain of RF-MS glass deposits, being overcome by multiple process methodologies. The sputtering pressure was shown as the most effective RF-MS parameter to accurately tailor/replication of source material composition and structure (with higher sputtering pressure being preferable) [47,80,94]. A long target pre-sputtering step (~45–60 min), under the same conditions used for the deposition of coatings, was equally important, as it led to significant improvement in the atomic target-to-substrate transfer [78–80]. The

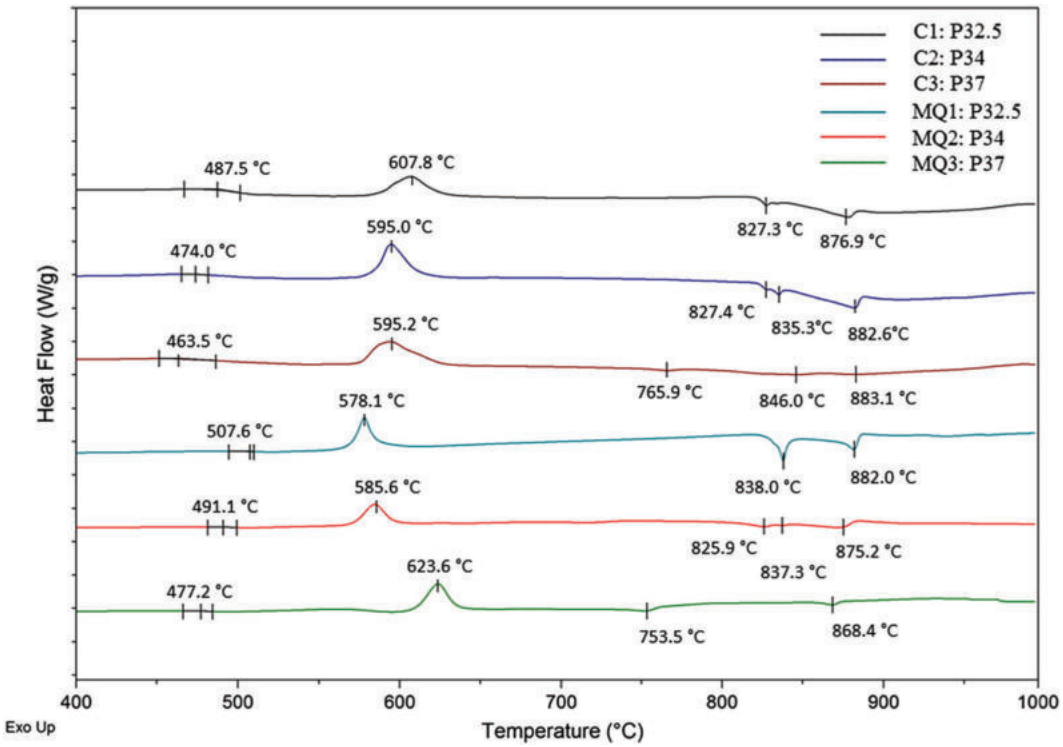

Fig. 15. DTA thermal traces for C1–C3 (deposited by RF-MS) and MQ1–MQ3. The T_g was determined at the onset of the primary endothermic peak. The peak locations of the T_c exothermic and T_m endothermic peaks have been also assessed. Reproduced with permission from Ref. [91].

pre-sputtering step balances the light–heavy elements ratios in the target surface, stabilizing it before starting the actual deposition process.

Of course, there is no universal RF-MS processing regime, with each target composition requiring definite process adjustments, but the indicative factors of influence have been now determined. On the other hand, the numerous available RF-MS variables (*e.g.*, sputtering pressure, working ambient, target-to-substrate distance, electrical power, or driving radio-frequency) permit finely tailoring the properties of the films while employing a single target composition (and therefore enable adaption of the mechanical and biological performances). This makes the process highly attractive and versatile from an economic standpoint.

Step and 3D features (with complex geometry and topology, such as dental implants) coverage is also no longer a burden and hindrance of RF-MS coating processes [55]. The simple translation/rotation of the substrate is a straightforward and efficient solution to overcome most shortcomings, furthermore the PVD industry has significantly evolved in the last decade, with numerous such technical solutions being already implemented in commercial systems.

The low deposition rate of RF-MS (generally at most of ~ 2–3 nm/min) has been increased by at least two times by the use of mildly "cold" pressed targets and a lower driving radio-frequency (than the customary 13.56 MHz) [47,89,94]. The use of powder targets, instead of the ubiquitous compact (melt-quenched into pre-forms or manufactured by sintering of compressed powders), heavily promoted by Stan & Ferreira and *et al.*, hold several definite advantages: (*i*) allows for employing higher target powers without the risk of irretrievably damaging/cracking the compact targets; (*ii*) enable reproducible coatings, since such targets can be simply reassembled before each deposition session (having a fresh target surface every time), and with that the modification of the surface composition of compact targets is circumvented.

In vitro testing of RF-MS SBG coatings showed noteworthy apatite-forming ability in both the inorganic SBF solution as well as in inorganic–organic cell culture media with increasing degrees of biomimicry, better replicating the human intercellular environment [80,89]. The designed morphological, compositional and structural modifications of the RF-MS PBG layers permitted engineering of their resorbability [91,94]. Noteworthy, very good cytocompatibility of both SBG and PBG sputtered films has been successfully shown in a large number of cell cultures, *e.g.*, human osteosarcoma MG63 [51] and Saos-2 [48,82,98], human primary osteoblast cells (hOB) [88], mouse fibroblast NIH/3T3 [77,81], human fibroblast Hs27 [82,94,95], human umbilical vein endothelial HUVEC [78], human dental pulp stem [55], or human mesenchymal stem [80,95] cell lines, demonstrating their readiness for further *in vivo* (on animal model) testing.

6. Future perspectives

Altogether, RF-MS seems to be a viable and highly-attractive option for bio-functionalizing a future generation of endosseous implants with BG layers. However, not all stones have been turned, and additional developments are needed with respect to RF-MS and other associated PVD techniques to: (*1*) further perfect characteristics of BG coatings (*i.e.*, surface topography will stimulate ideal cell adhesion which in turn will increase osseointegration; increase of wettability will improve initial protein adhesion, a primary factor for biological performance); (*2*) delineate definite technical specifications for BG coatings (*e.g.*, effect of sterilization techniques on their mechanical and biological performances is unknown; a critical coating thickness was not determined to date, regardless of deposition technology); (*3*) add new bio-functional traits (*e.g.*, as the "post-antibiotic era" has begun, with super bacteria resistant to all drugs, and thus, thus requiring identification of complimentary groups of ionic therapeutic agents, which can boost and expand the antimicrobial range of BG); (*4*) implement solutions for increasing the deposition rate, and by that reduce the time required for RF-MS coating which will allow for greater manufacturability and a smooth translation to the clinic (*e.g.*, further investigation into electron beam evaporation of BGs could be a significant step towards achieving orders of magnitude increases in deposition); (*5*) trial techniques such as HiPIMS and other ionised PVD systems to improve coverage of high aspect ratio substrate features such as coatings on scaffolds; and (*6*)

increase the area of uniformity by employing larger-sized magnetron cathode deposition systems, with higher costs than the laboratory-grade ones, but better-fitting in an industrial scenario. Furthermore, the devitrification (by post-deposition annealing treatments) of SBGs and PBGs as routes for improving their mechanical performance and engineering their degradability in body fluids has been rarely explored, whilst the BBGs (currently ascending as highly promising biomaterials) have never been deposited by RF-MS, this field of research remaining *terra incognita* to date.

Regardless of type (SBG, PBG, BBG or hybrid), all research efforts need to be linked to a clear vision on the future industrialisation of physical vapour deposited implant-type coatings. This review has highlighted a noteworthy acceleration in the field of sputtered BGs. Within the public domain, the focus has been limited to R&D scale proof of concept manufacturing, manipulation of the process variables and their influence on structural properties, compositional tailor-ability, and mechanical properties. *In vitro* efficacy relating to apatite-forming ability (SBGs case), controlled resorbability (PBGs case), cytocompatibility, and antimicrobial traits have been demonstrated. It has been shown here that RF-MS can apply BG thin-films on medical implants to the same effect as the tens of thousands of studies on MQ glasses since L. L. Hench created first BG in the early 1970s. Two decades of work in this area have produced tens of publications on RF-MS/PVD deposited BGs, bringing us to an inflection point whereby the future direction should be (*1*) steered towards bridging the commercial gap and aiming to prove industrial potential of BG thin-films by developing their compatibility with high deposition rate, cost effective PVD technologies; and (*2*) taking steps towards regulatory approval and industry wide adoption as a future replacement for conventional orthopaedic coatings.

The path towards industrialisation of thin-film materials is decades ahead in the semiconductor, solar and battery industries, and thus, lessons are available to be assimilated. Some examples include lithium phosphate oxynitride as a solid-state battery electrolyte fabricated by e-beam plasma assisted deposition, an industrial evaporation method capable of microns per minute rates, suggesting that PBGs may be as well successfully applied by high-rate methodologies [143]. Similarly, SiO_2 amorphous structures were successfully deposited as optical films by e-beam evaporation in the early 1990s [144]. Whilst production rates of BG films may be vastly increased by other methods, it is often at the expense of the control offered by RF-MS, with this as a consideration, less conventional, novel manufacturing methods such as remote plasma sputtering has been shown to offer the control of conventional sputtering, whilst showing ability to deposit amorphous films such as indium tin oxide, at enhanced rates, with benefits for thermal management over amorphous and ceramic targets [145]. It is our belief that future is in pushing the boundaries of manufacturing compatibility with such methods and by making novel developments to enable the industrialisation of BG coatings.

CRediT authorship contribution statement

George E. Stan: Conceptualization, Methodology, Data curation, Writing – original draft, Writing – review & editing, Supervision, Funding acquisition. **Maziar Montazerian:** Conceptualization, Writing – original draft. **Adam Shearer:** Writing – original draft. **Bryan W. Stuart:** Conceptualization, Writing – original draft, Writing – review & editing. **Francesco Baino:** Writing – review & editing, Supervision, Funding acquisition. **John C. Mauro:** Writing – review & editing, Supervision. **José M.F. Ferreira:** Conceptualization, Writing – review & editing, Supervision, Funding acquisition.

Declaration of Competing Interest

The authors declare that they have no known competing financial interests or personal relationships that could have appeared to influence the work reported in this paper.

Data availability

No data was used for the research described in the article.

Acknowledgement

The POLONEZ BIS 1 “BAGBONE”, Project no. 536651 supported by the Polish National Science Centre is acknowledged by JMFF. GES thanks to the Core Program of the National Institute of Materials Physics within the National Research Development and Innovation Plan 2022–2027, carried out with the support of the Romanian Ministry of Research, Innovation and Digitalization under the project PC1-PN23080101.

References

[1] Grand-View-Research, Dental implants market size, share & trends analysis report, (2023). https://www.grandviewresearch.com/industry-analysis/dental-implants-market?utm_source=prnewswire&utm_medium=referral&utm_campaign=hc_25-oct-22&utm_term=dental-implants-market&utm_content=rd1 (accessed July 9, 2023).
[2] M. Montazerian, F. Hosseinzadeh, C. Migneco, M.V.L. Fook, F. Baino, Bioceramic coatings on metallic implants: An overview, Ceram. Int. 48 (2022) 8987–9005, https://doi.org/10.1016/j.ceramint.2022.02.055.
[3] V. Miguez-Pacheco, L.L. Hench, A.R. Boccaccini, Bioactive glasses beyond bone and teeth: Emerging applications in contact with soft tissues, Acta Biomater. 13 (2015) 1–15, https://doi.org/10.1016/j.actbio.2014.11.004.
[4] M. Montazerian, F. Baino, E. Fiume, C. Migneco, A. Alaghmandfard, O. Sedighi, A.V. DeCeanne, C.J. Wilkinson, J.C. Mauro, Glass-ceramics in dentistry: Fundamentals, technologies, experimental techniques, applications, and open issues, Prog. Mater. Sci. 132 (2023), 101023, https://doi.org/10.1016/j.pmatsci.2022.101023.
[5] Y. Zhao, C. Chen, D. Wang, The current techniques for preparing bioglass coatings, Surf. Rev. Lett. 12 (2005) 505–513, https://doi.org/10.1142/S0218625X05007347.
[6] A. Sola, D. Bellucci, V. Cannillo, A. Cattini, Bioactive glass coatings: A review, Surf. Eng. 27 (2011) 560–572, https://doi.org/10.1179/1743294410Y.0000000008.
[7] E. Verné, Bioactive glass and glass-ceramic coatings, in: J.R. Jones, A.G. Clare (Eds.), Bio-Glasses, 1st ed.,, Wiley, Hoboken, NJ, USA, 2012, pp. 107–119, https://doi.org/10.1002/9781118346457.ch8.
[8] F. Baino, E. Verne, Glass-based coatings on biomedical implants: A state-of-the-art review, Biomed. Glas. 3 (2017) 1–17, https://doi.org/10.1515/bglass-2017-0001.
[9] R. Sergi, D. Bellucci, V. Cannillo, A comprehensive review of bioactive glass coatings: State of the art, challenges and future perspectives, Coatings. 10 (2020) 757, https://doi.org/10.3390/coatings10080757.
[10] J.N. Oliver, Y. Su, X. Lu, P.-H. Kuo, J. Du, D. Zhu, Bioactive glass coatings on metallic implants for biomedical applications, Bioact. Mater. 4 (2019) 261–270, https://doi.org/10.1016/j.bioactmat.2019.09.002.
[11] F. Baino, M.A. Montealegre, G. Orlygsson, G. Novajra, C. Vitale-Brovarone, Bioactive glass coatings fabricated by laser cladding on ceramic acetabular cups: a proof-of-concept study, J. Mater. Sci. 52 (2017) 9115–9128, https://doi.org/10.1007/s10853-017-0837-8.
[12] R.B. Heimann, Plasma-sprayed hydroxylapatite coatings as biocompatible intermediaries between inorganic implant surfaces and living tissue, J. Therm. Spray Technol. 27 (2018) 1212–1237, https://doi.org/10.1007/s11666-018-0737-8.
[13] T. Tite, A.C. Popa, L.M. Balescu, I.M. Bogdan, I. Pasuk, J.M.F. Ferreira, G.E. Stan, Cationic substitutions in hydroxyapatite: Current status of the derived biofunctional effects and their in vitro interrogation methods, Materials (Basel). 11 (2018) 2081, https://doi.org/10.3390/ma11112081.
[14] T. Callahan, J. Gantenberg, B. Sands, Calcium phosphate (Ca-P) coating draft guidance for preparation of Food and Drug Administration (FDA) submissions for orthopedic and dental endosseous implants, in: Charact. Perform. Calcium Phosphate Coatings Implant., ASTM International, West Conshohocken, PA, USA, 1994: pp. 185–197. doi:10.1520/STP25193S.
[15] G. Goller, The effect of bond coat on mechanical properties of plasma sprayed bioglass-titanium coatings, Ceram. Int. 30 (2004) 351–355, https://doi.org/10.1016/S0272-8842(03)00107-X.
[16] V. López Calvo, M. Vicent Cabedo, E. Bannier, E. Cañas Recacha, A.R. Boccaccini, L. Cordero Arias, E., Sánchez Vilches, 45S5 bioactive glass coatings by atmospheric plasma spraying obtained from feedstocks prepared by different routes, J. Mater. Sci. 49 (2014) 7933–7942, https://doi.org/10.1007/s10853-014-8519-2.
[17] Y. Xiao, L. Song, X. Liu, Y. Huang, T. Huang, Y. Wu, J. Chen, F. Wu, Nanostructured bioactive glass–ceramic coatings deposited by the liquid precursor plasma spraying process, Appl. Surf. Sci. 257 (2011) 1898–1905, https://doi.org/10.1016/j.apsusc.2010.09.023.
[18] Y. Xiao, L. Song, X. Liu, Y. Huang, T. Huang, J. Chen, Y. Wu, F. Wu, Bioactive glass-ceramic coatings synthesized by the liquid precursor plasma spraying

process, J. Therm. Spray Technol. 20 (2011) 560–568, https://doi.org/10.1007/s11666-010-9594-9.
[19] A. Cattini, L. Łatka, D. Bellucci, G. Bolelli, A. Sola, L. Lusvarghi, L. Pawłowski, V. Cannillo, Suspension plasma sprayed bioactive glass coatings: Effects of processing on microstructure, mechanical properties and in-vitro behaviour, Surf. Coatings Technol. 220 (2013) 52–59, https://doi.org/10.1016/j.surfcoat.2012.10.076.
[20] E. Cañas, M. Vicent, M.J. Orts, R. Moreno, E. Sánchez, Bioactive glass suspensions preparation for suspension plasma spraying, J. Eur. Ceram. Soc. 36 (2016) 4281–4290, https://doi.org/10.1016/j.jeurceramsoc.2016.06.011.
[21] L. Altomare, D. Bellucci, G. Bolelli, B. Bonferroni, V. Cannillo, L. De Nardo, R. Gadow, A. Killinger, L. Lusvarghi, A. Sola, N. Stiegler, Microstructure and in vitro behaviour of 45S5 bioglass coatings deposited by high velocity suspension flame spraying (HVSFS), J. Mater. Sci. Mater. Med. 22 (2011) 1303–1319, https://doi.org/10.1007/s10856-011-4307-6.
[22] M. Monsalve, E. Lopez, H. Ageorges, F. Vargas, Bioactivity and mechanical properties of bioactive glass coatings fabricated by flame spraying, Surf. Coatings Technol. 268 (2015) 142–146, https://doi.org/10.1016/j.surfcoat.2014.08.041.
[23] S. Bano, I. Ahmed, D.M. Grant, A. Nommeots-Nomm, T. Hussain, Effect of processing on microstructure, mechanical properties and dissolution behaviour in SBF of Bioglass (45S5) coatings deposited by Suspension High Velocity Oxy Fuel (SHVOF) thermal spray, Surf. Coatings Technol. 372 (2019) 229–238, https://doi.org/10.1016/j.surfcoat.2019.05.038.
[24] B. Garrido, V. Albaladejo-Fuentes, I.G. Cano, S. Dosta, Development of bioglass/PEEK composite coating by cold gas spray for orthopedic implants, J. Therm. Spray Technol. 31 (2022) 186–196, https://doi.org/10.1007/s11666-021-01312-w.
[25] B. Garrido, S. Dosta, I.G. Cano, Bioactive glass coatings obtained by thermal spray: Current status and future challenges, Boletín La Soc, Española Cerámica y Vidr. 61 (2022) 516–530, https://doi.org/10.1016/j.bsecv.2021.04.001.
[26] A. Woźniak, M. Staszuk, Ł. Reimann, O. Bialas, Z. Brytan, S. Voinarovych, O. Kyslytsia, S. Kaliuzhnyi, M. Basiaga, M. Admiak, The influence of plasma-sprayed coatings on surface properties and corrosion resistance of 316L stainless steel for possible implant application, Arch. Civ. Mech. Eng. 21 (2021) 148, https://doi.org/10.1007/s43452-021-00297-1.
[27] M. Bosetti, E. Vernè, M. Ferraris, A. Ravaglioli, M. Cannas, In vitro characterisation of zirconia coated by bioactive glass, Biomaterials. 22 (2001) 987–994, https://doi.org/10.1016/S0142-9612(00)00264-7.
[28] S. Fujino, H. Tokunaga, E. Saiz, A.P. Tomsia, Fabrication and characterization of bioactive glass coatings on Co-Cr implant alloys, Mater. Trans. 45 (2004) 1147–1151, https://doi.org/10.2320/matertrans.45.1147.
[29] S. Lopez-Esteban, E. Saiz, S. Fujino, T. Oku, K. Suganuma, A.P. Tomsia, Bioactive glass coatings for orthopedic metallic implants, J. Eur. Ceram. Soc. 23 (2003) 2921–2930, https://doi.org/10.1016/S0955-2219(03)00303-0.
[30] V. Stanic, N. Nicoli Aldini, M. Fini, G. Giavaresi, R. Giardino, A. Krajewski, A. Ravaglioli, M. Mazzocchi, B. Dubini, M. Ponzi Bossi, F. Rustichelli, Osteointegration of bioactive glass-coated zirconia in healthy bone: an in vivo evaluation, Biomaterials. 23 (2002) 3833–3841, https://doi.org/10.1016/S0142-9612(02)00119-9.
[31] D. Krause, B. Thomas, C. Leinenbach, D. Eifler, E.J. Minay, A.R. Boccaccini, The electrophoretic deposition of Bioglass® particles on stainless steel and Nitinol substrates, Surf. Coatings Technol. 200 (2006) 4835–4845, https://doi.org/10.1016/j.surfcoat.2005.04.029.
[32] M. Mehdipour, A. Afshar, M. Mohebali, Electrophoretic deposition of bioactive glass coating on 316L stainless steel and electrochemical behavior study, Appl. Surf. Sci. 258 (2012) 9832–9839, https://doi.org/10.1016/j.apsusc.2012.06.038.
[33] K. Kawaguchi, M. Iijima, K. Endo, I. Mizoguchi, Electrophoretic deposition as a new bioactive glass coating process for orthodontic stainless steel, Coatings. 7 (2017) 199, https://doi.org/10.3390/coatings7110199.
[34] M. Hamadouche, A. Meunier, D.C. Greenspan, C. Blanchat, J.P. Zhong, G.P. La Torre, L. Sedel, Bioactivity of sol-gel bioactive glass coated alumina implants, J. Biomed. Mater. Res. 52 (2000) 422–429, https://doi.org/10.1002/1097-4636(200011)52:2<422::AID-JBM24>3.0.CO;2-P.
[35] P.P. Singh, K. Dixit, N. Sinha, A sol-gel based bioactive glass coating on laser textured 316L stainless steel substrate for enhanced biocompatability and anti-corrosion properties, Ceram. Int. 48 (2022) 18704–18715, https://doi.org/10.1016/j.ceramint.2022.03.144.
[36] L. D'Alessio, R. Teghil, M. Zaccagnino, I. Zaccardo, D. Ferro, V. Marotta, Pulsed laser ablation and deposition of bioactive glass as coating material for biomedical applications, Appl. Surf. Sci. 138–139 (1999) 527–532, https://doi.org/10.1016/S0169-4332(98)00610-2.
[37] Y. Zhao, M. Song, C. Chen, J. Liu, The role of the pressure in pulsed laser deposition of bioactive glass films, J. Non. Cryst. Solids. 354 (2008) 4000–4004, https://doi.org/10.1016/j.jnoncrysol.2008.05.019.
[38] L. Floroian, B. Savu, G. Stanciu, A.C. Popescu, F. Sima, I.N. Mihailescu, R. Mustata, L.E. Sima, S.M. Petrescu, D. Tanaskovic, D. Janackovic, Nanostructured bioglass thin films synthesized by pulsed laser deposition: CSLM, FTIR investigations and in vitro biotests, Appl. Surf. Sci. 255 (2008) 3056–3062, https://doi.org/10.1016/j.apsusc.2008.08.105.
[39] J.V. Rau, R. Teghil, M. Fosca, A. De Bonis, I. Cacciotti, A. Bianco, V.R. Albertini, R. Caminiti, A. Ravaglioli, Bioactive glass–ceramic coatings prepared by pulsed laser deposition from RKKP targets (sol–gel vs melt-processing route), Mater. Res. Bull. 47 (2012) 1130–1137, https://doi.org/10.1016/j.materresbull.2012.02.011.
[40] D. Bellucci, M. Bianchi, G. Graziani, A. Gambardella, M. Berni, A. Russo, V. Cannillo, Pulsed electron deposition of nanostructured bioactive glass coatings for biomedical applications, Ceram. Int. 43 (2017) 15862–15867, https://doi.org/10.1016/j.ceramint.2017.08.159.
[41] A. Liguori, C. Gualandi, M.L. Focarete, F. Biscarini, M. Bianchi, The pulsed electron deposition technique for biomedical applications: A review, Coatings. 10 (2020), https://doi.org/10.3390/coatings10010016.
[42] L.L. Hench, J. Wilson, P. Ruzakowski, Final report to NASA-Lewis Research Center "Ion beam sputtered coatings of bioglass", 1st of March 1982, (n.d.). https://ntrs.nasa.gov/search.jsp?R=19910019070 (accessed June 14, 2023).
[43] C.X. Wang, Z.Q. Chen, M. Wang, Fabrication and characterization of bioactive glass coatings produced by the ion beam sputter deposition technique, J. Mater. Sci. Mater. Med. 13 (2002) 247–251, https://doi.org/10.1023/A:1014050715535.
[44] C.C. Mardare, A.I. Mardare, J.R.F. Fernandes, E. Joanni, S.C.A. Pina, M.H. V. Fernandes, R.N. Correia, Deposition of bioactive glass-ceramic thin-films by RF magnetron sputtering, J. Eur. Ceram. Soc. 23 (2003) 1027–1030, https://doi.org/10.1016/S0955-2219(02)00278-9.
[45] J.G.C. Wolke, E. Vandenbulcke, B. van Oirschot, J.A. Jansen, A study to the surface characteristics of RF magnetron sputtered bioglass - and calcium phosphate coatings, Key Eng. Mater. 284–286 (2005) 187–190, https://doi.org/10.4028/www.scientific.net/KEM.284-286.187.
[46] A. Slav, A. Ianculescu, C. Morosanu, A. Saranti, I. Koutselas, S. Agathopoulos, M. A. Karakassides, Rough bioglass films prepared by magnetron sputtering, Key Eng. Mater. 361–363 (2008) 245–248, https://doi.org/10.4028/www.scientific.net/KEM.361-363.245.
[47] G.E. Stan, C.O. Morosanu, D.A. Marcov, I. Pasuk, F. Miculescu, G. Reumont, Effect of annealing upon the structure and adhesion properties of sputtered bio-glass/titanium coatings, Appl. Surf. Sci. 255 (2009) 9132–9138, https://doi.org/10.1016/j.apsusc.2009.06.117.
[48] E. Saino, V. Maliardi, E. Quartarone, L. Fassina, L. Benedetti, M.G.C. De Angelis, P. Mustarelli, A. Facchini, L. Visai, In vitro enhancement of SAOS-2 cell calcified matrix deposition onto radio frequency magnetron sputtered bioglass-coated titanium scaffolds, Tissue Eng. Part A 16 (2010) 995–1008, https://doi.org/10.1089/ten.tea.2009.0051.
[49] G.E. Stan, A.C. Popa, A.C. Galca, G. Aldica, J.M.F. Ferreira, Strong bonding between sputtered bioglass-ceramic films and Ti-substrate implants induced by atomic inter-diffusion post-deposition heat-treatments, Appl. Surf. Sci. 280 (2013) 530–538, https://doi.org/10.1016/j.apsusc.2013.05.022.
[50] B. Stuart, M. Gimeno-Fabra, J. Segal, I. Ahmed, D.M. Grant, Preferential sputtering in phosphate glass systems for the processing of bioactive coatings, Thin Solid Films. 589 (2015) 534–542, https://doi.org/10.1016/j.tsf.2015.05.072.
[51] J.K. Bibby, N.L. Bubb, D.J. Wood, P.M. Mummery, Fluorapatite-mullite glass sputter coated Ti6Al4V for biomedical applications, J. Mater. Sci. Mater. Med. 16 (2005) 379–385, https://doi.org/10.1007/s10856-005-6975-6.
[52] J. Schrooten, J. Helsen, Adhesion of bioactive glass coating to Ti6Al4V oral implant, Biomaterials. 21 (2000) 1461–1469, https://doi.org/10.1016/S0142-9612(00)00027-2.
[53] N. Drnovšek, S. Novak, U. Dragin, M. Čeh, M. Gorenšek, M. Gradišar, Bioactive glass enhances bone ingrowth into the porous titanium coating on orthopaedic implants, Int. Orthop. 36 (2012) 1739–1745, https://doi.org/10.1007/s00264-012-1520-y.
[54] B.A.J.A. Van Oirschot, H.S. Alghamdi, T.O. Närhi, S. Anil, A. Al Farraj Aldosari, J. J.J.P. Van den Beucken, J.A. Jansen, In vivo evaluation of bioactive glass-based coatings on dental implants in a dog implantation model, Clin. Oral Implants Res. 25 (2014) 21–28. doi:10.1111/clr.12060.
[55] A.C. Popa, G.E. Stan, M. Enculescu, C. Tanase, D.U. Tulyaganov, J.M.F. Ferreira, Superior biofunctionality of dental implant fixtures uniformly coated with durable bioglass films by magnetron sputtering, J. Mech. Behav. Biomed. Mater. 51 (2015) 313–327, https://doi.org/10.1016/j.jmbbm.2015.07.028.
[56] B.A.J.A. van Oirschot, G.J. Meijer, E.M. Bronkhorst, T. Närhi, J.A. Jansen, J.J.J. P. van den Beucken, Comparison of different surface modifications for titanium implants installed into the goat iliac crest, Clin. Oral Implants Res. 27 (2016) e57–e67, https://doi.org/10.1111/clr.12529.
[57] J. Mesquita-Guimarães, B. Henriques, F.S. Silva, Bioactive glass coatings, in: H.B. T.-B.G. (Second E. Ylänen (Ed.), Bioact. Glas., Elsevier, 2018: pp. 103–118. doi:10.1016/B978-0-08-100936-9.00007-1.
[58] C.Z. Chen, X.G. Meng, H.J. Yu, H. Yang, T. He, D.G. Wang, S.G. Zhao, A review of coating preparing techniques of bioactive glass, Adv. Mater. Res. 833 (2013) 202–207, https://doi.org/10.4028/www.scientific.net/AMR.833.202.
[59] H.R. Fernandes, A. Gaddam, A. Rebelo, D. Brazete, G.E. Stan, J.M.F.F. Ferreira, Bioactive glasses and glass-ceramics for healthcare applications in bone regeneration and tissue engineering, Materials (Basel). 11 (2018) 2530, https://doi.org/10.3390/ma11122530.
[60] J. Chang, Y.L. Zhou, Surface modification of bioactive glasses, in: H.B.T.-B.G. (Second E. Ylänen (Ed.), Bioact. Glas., Elsevier, 2018: pp. 119–143. doi:10.1016/B978-0-08-100936-9.00008-3.
[61] M. Maximov, O.-C. Maximov, L. Craciun, D. Ficai, A. Ficai, E. Andronescu, Bioactive glass—An extensive study of the preparation and coating methods, Coatings. 11 (2021) 1386, https://doi.org/10.3390/coatings11111386.
[62] L.L. Hench, The story of Bioglass®, J. Mater. Sci. Mater. Med. 17 (2006) 967–978, https://doi.org/10.1007/s10856-006-0432-z.
[63] G. Piotrowski, L.L. Hench, W.C. Allen, G.J. Miller, Mechanical studies of the bone bioglass interfacial bond, J. Biomed. Mater. Res. 9 (1975) 47–61, https://doi.org/10.1002/jbm.820090408.
[64] P. Griss, D.C. Greenspan, G. Heimke, B. Krempien, R. Buchinger, L.L. Hench, G. Jentschura, Evaluation of a bioglass-coated Al2O3 total hip prosthesis in

sheep, J. Biomed. Mater. Res. 10 (1976) 511–518, https://doi.org/10.1002/jbm.820100406.
[65] D.C. Greenspan, L.L. Hench, Chemical and mechanical behavior of bioglass-coated alumina, J. Biomed. Mater. Res. 10 (1976) 503–509, https://doi.org/10.1002/jbm.820100405.
[66] P. Ducheyne, L.L. Hench, P. de Meester, Short term bonding behaviour of bioglass coatings on metal substrate, J. Biomech. 13 (1980) 807–808, https://doi.org/10.1016/0021-9290(80)90302-4.
[67] D.M. Mattox, Physical sputtering and sputter deposition (Sputtering), in: D.M.B. T.-H. of P.V.D. (PVD) P. (Second E. Mattox (Ed.), Handb. Phys. Vap. Depos. Process., Elsevier, Boston, 2010: pp. 237–286. doi:10.1016/B978-0-8155-2037-5.00007-1.
[68] F.M. Penning, The spark discharge in low pressure between coaxial cylinders in an axial magnet field, Physica. 3 (1936) 873–894.
[69] S. Schiller, U. Heisig, K. Goedicke, Use of the ring gap plasmatron for high rate sputtering, Thin Solid Films. 40 (1977) 327–334, https://doi.org/10.1016/0040-6090(77)90134-1.
[70] J. Chapin, Sputtering process and apparatus (1974).
[71] T. Welzel, K. Ellmer, Comparison of ion energies and fluxes at the substrate during magnetron sputtering of ZnO : Al for dc and rf discharges, J. Phys. D. Appl. Phys. 46 (2013), 315202, https://doi.org/10.1088/0022-3727/46/31/315202.
[72] R.S. Nowicki, Properties of rf-sputtered Al2O3 films deposited by planar magnetron, J. Vac. Sci. Technol. 14 (1977) 127–133, https://doi.org/10.1116/1.569103.
[73] S. Swann, Magnetron sputtering, Phys. Technol. 19 (1988) 67–75, https://doi.org/10.1088/0305-4624/19/2/304.
[74] K. Wasa, I. Kanno, H. Kotera, Handbook of Sputtering Technology, Elsevier (2012), https://doi.org/10.1016/C2010-0-67037-4.
[75] P.N. Hishimone, H. Nagai, M. Sato, Methods of fabricating thin films for energy materials and devices, in: M. Sato, L. Lu, H. Nagai (Eds.), Lithium-Ion Batter. - Thin Film. Energy Mater. Devices, IntechOpen, Rijeka, 2020: p. Ch. 2. doi: 10.5772/intechopen.85912.
[76] C. Berbecaru, G.E. Stan, S. Pina, D.U. Tulyaganov, J.M.F. Ferreira, The bioactivity mechanism of magnetron sputtered bioglass thin films, Appl. Surf. Sci. 258 (2012) 9840–9848, https://doi.org/10.1016/j.apsusc.2012.06.039.
[77] A.C. Popa, V.M.F. Marques, G.E. Stan, M.A. Husanu, A.C. Galca, C. Ghica, D. U. Tulyaganov, A.F. Lemos, J.M.F. Ferreira, Nanomechanical characterization of bioglass films synthesized by magnetron sputtering, Thin Solid Films. 553 (2014) 166–172, https://doi.org/10.1016/j.tsf.2013.10.104.
[78] A.C. Popa, G.E. Stan, C. Besleaga, L. Ion, V.A. Maraloiu, D.U. Tulyaganov, J.M. F. Ferreira, Submicrometer hollow bioglass cones deposited by radio frequency magnetron sputtering: Formation mechanism, properties, and prospective biomedical applications, ACS Appl. Mater. Interfaces. 8 (2016) 4357–4367, https://doi.org/10.1021/acsami.6b00606.
[79] A.I. Bita, G.E. Stan, M. Niculescu, I. Ciuca, E. Vasile, I. Antoniac, Adhesion evaluation of different bioceramic coatings on Mg-Ca alloys for biomedical applications, J. Adhes. Sci. Technol. 30 (2016) 1968–1983, https://doi.org/10.1080/01694243.2016.1171569.
[80] A.C. Popa, G.E. Stan, M.A. Husanu, I. Mercioniu, L.F. Santos, H.R. Fernandes, J.M. F. Ferreira, Bioglass implant-coating interactions in synthetic physiological fluids with varying degrees of biomimicry, Int. J. Nanomedicine. 12 (2017) 683–707, https://doi.org/10.2147/IJN.S123236.
[81] G.E. Stan, T. Tite, A.-C. Popa, I.M. Chirica, C.C. Negrila, C. Besleaga, I. Zgura, A. C. Sergentu, G. Popescu-Pelin, D. Cristea, L.E. Ionescu, M. Necsulescu, H. R. Fernandes, J.M.F. Ferreira, The beneficial mechanical and biological outcomes of thin copper-gallium doped silica-rich bio-active glass implant-type coatings, Coatings. 10 (2020) 1119, https://doi.org/10.3390/coatings10111119.
[82] A.-I. Bița, I. Antoniac, M. Miculescu, G.E. Stan, L. Leonat, A. Antoniac, B. Constantin, N. Forna, Electrochemical and in vitro biological evaluation of bio-Active coatings deposited by magnetron sputtering onto biocompatible Mg-0.8Ca alloy, Materials (Basel) 15 (2022) 3100, https://doi.org/10.3390/ma15093100.
[83] G.E. Stan, S. Pina, D.U. Tulyaganov, J.M.F. Ferreira, I. Pasuk, C.O. Morosanu, Biomineralization capability of adherent bio-glass films prepared by magnetron sputtering, J. Mater. Sci. Mater. Med. 21 (2010) 1047–1055, https://doi.org/10.1007/s10856-009-3940-9.
[84] C. Berbecaru, H.V. Alexandru, G.E. Stan, D.A. Marcov, I. Pasuk, A. Ianculescu, First stages of bioactivity of glass-ceramics thin films prepared by magnetron sputtering technique, Mater. Sci. Eng. B Solid-State Mater. Adv. Technol. 169 (2010) 101–105, https://doi.org/10.1016/j.mseb.2010.01.007.
[85] G.E. Stan, A.C. Popa, D. Bojin, Bioreactivity evaluation in simulated body fluid of magnetron sputtered glass and glass-ceramic coatings: A FTIR spectroscopy study, Dig. J. Nanomater. Biostructures. 5 (2010) 557–566.
[86] G.E. Stan, D. Bojin, Adherent glass-ceramic thin layers with bioactive potential deposited by magnetron sputtering techniques, UPB Sci, Bull. Ser. B Chem. Mater. Sci. 72 (2010) 187–196.
[87] G.E. Stan, D.A. Marcov, I. Pasuk, F. Miculescu, S. Pina, D.U. Tulyaganov, J.M. F. Ferreira, Bioactive glass thin films deposited by magnetron sputtering technique: The role of working pressure, Appl. Surf. Sci. 256 (2010) 7102–7110, https://doi.org/10.1016/j.apsusc.2010.05.035.
[88] G.E. Stan, A.C. Popescu, I.N. Mihailescu, D.A. Marcov, R.C. Mustata, L.E. Sima, S. M. Petrescu, A. Ianculescu, R. Trusca, C.O. Morosanu, On the bioactivity of adherent bioglass thin films synthesized by magnetron sputtering techniques, Thin Solid Films. 518 (2010) 5955–5964, https://doi.org/10.1016/j.tsf.2010.05.104.
[89] G.E. Stan, I. Pasuk, M.A. Husanu, I. Enculescu, S. Pina, A.F. Lemos, D. U. Tulyaganov, K. El Mabrouk, J.M.F. Ferreira, Highly adherent bioactive glass thin films synthetized by magnetron sputtering at low temperature, J. Mater. Sci. Mater. Med. 22 (2011) 2693–2710, https://doi.org/10.1007/s10856-011-4441-1.
[90] B.W. Stuart, M. Gimeno-Fabra, J. Segal, I. Ahmed, D.M. Grant, Degradation and characterization of resorbable phosphate-based glass thin-film coatings applied by radio-frequency magnetron sputtering, ACS Appl. Mater. Interfaces. 7 (2015) 27362–27372, https://doi.org/10.1021/acsami.5b08957.
[91] B.W. Stuart, J.J. Titman, M. Gimeno-Fabra, I. Ahmed, D.M. Grant, Insights into structural characterisation and thermal properties of compositionally equivalent vapour-condensed and melt-quenched glasses, Mater. Des. 111 (2016) 174–184, https://doi.org/10.1016/j.matdes.2016.08.063.
[92] B.W. Stuart, M. Gimeno-Fabra, J. Segal, I. Ahmed, D.M. Grant, Mechanical, structural and dissolution properties of heat treated thin-film phosphate based glasses, Appl. Surf. Sci. 416 (2017) 605–617, https://doi.org/10.1016/j.apsusc.2017.04.110.
[93] B.W. Stuart, C.A. Grant, G.E. Stan, A.C. Popa, J.J. Titman, D.M. Grant, Gallium incorporation into phosphate based glasses: Bulk and thin film properties, J. Mech. Behav. Biomed. Mater. 82 (2018) 371–382, https://doi.org/10.1016/j.jmbbm.2018.03.041.
[94] T. Tite, A.C. Popa, I.M. Chirica, B.W. Stuart, A.C. Galca, L.M. Balescu, G. Popescu-Pelin, D.M. Grant, J.M.F. Ferreira, G.E. Stan, Phosphate bioglass thin-films: Cross-area uniformity, structure and biological performance tailored by the simple modification of magnetron sputtering gas pressure, Appl. Surf. Sci. 541 (2021), 148640, https://doi.org/10.1016/j.apsusc.2020.148640.
[95] B.W. Stuart, G.E. Stan, A.C. Popa, M.J. Carrington, I. Zgura, M. Necsulescu, D. M. Grant, New solutions for combatting implant bacterial infection based on silver nano-dispersed and gallium incorporated phosphate bioactive glass sputtered films: A preliminary study, Bioact. Mater. 8 (2022) 325–340, https://doi.org/10.1016/j.bioactmat.2021.05.055.
[96] M. Iijima, M. Hashimoto, N. Kohda, S. Nakagaki, T. Muguruma, K. Endo, I. Mizoguchi, Crystal growth on bioactive glass sputter-coated alumina in artificial saliva, Dent. Mater. J. 32 (2013) 775–780, https://doi.org/10.4012/dmj.2013-120.
[97] M. Iijima, M. Hashimoto, S. Nakagaki, T. Muguruma, N. Kohda, K. Endo, I. Mizoguchi, Bioactive glass coating of orthodontic material for the recovery of mechanical properties of etched enamel, J. Biomater. Tissue Eng. 4 (2014) 274–280, https://doi.org/10.1166/jbt.2014.1171.
[98] P.S. Sato, T. Watanabe, H. Maeda, A. Obata, T. Kasuga, Preparation of an antibacterial amorphous thin film by radiofrequency magnetron sputtering using a 65ZnO–30P2O5–5Nb2O5 glass, J. Non. Cryst. Solids. 528 (2020), 119724, https://doi.org/10.1016/j.jnoncrysol.2019.119724.
[99] S.-B. Cho, K. Nakanishi, T. Kokubo, N. Soga, C. Ohtsuki, T. Nakamura, T. Kitsugi, T. Yamamuro, Dependence of apatite formation on silica gel on its structure: Effect of heat treatment, J. Am. Ceram. Soc. 78 (1995) 1769–1774, https://doi.org/10.1111/j.1151-2916.1995.tb08887.x.
[100] International Organization for Standardization, ISO 13779–2:2018 Implants for surgery — Hydroxyapatite — Part 2: Thermally sprayed coatings of hydroxyapatite, Switz, Geneva, 2018 https://www.iso.org/standard/64617.html (accessed June 17, 2023.
[101] D. Bellucci, V. Cannillo, A. Sola, Coefficient of thermal expansion of bioactive glasses: Available literature data and analytical equation estimates, Ceram. Int. 37 (2011) 2963–2972, https://doi.org/10.1016/j.ceramint.2011.05.048.
[102] P. Hidnert, Thermal expansion of titanium, J. Res. Natl. Bur. Stand. 30 (1943) (1934) 101, https://doi.org/10.6028/jres.030.008.
[103] AZO-Materials, Ti6Al4V alloy properties, (n.d.). https://www.azom.com/article.aspx?ArticleID=1547 (accessed June 17, 2023).
[104] AZO-Materials, Ti6Al7Nb alloy properties, (n.d.). https://www.azom.com/properties.aspx?ArticleID=2064 (accessed June 17, 2023).
[105] L.L. Hench, Bioceramics: From concept to clinic, J. Am. Ceram. Soc. 74 (1991) 1487–1510, https://doi.org/10.1111/j.1151-2916.1991.tb07132.x.
[106] R.S. Pryce, L.L. Hench, Dissolution characteristics of bioactive glasses, Key Eng. Mater. 240–242 (2003) 201–204, https://doi.org/10.4028/www.scientific.net/kem.240-242.201.
[107] F.E. Ciraldo, E. Boccardi, V. Melli, F. Westhauser, A.R. Boccaccini, Tackling bioactive glass excessive in vitro bioreactivity: Preconditioning approaches for cell culture tests, Acta Biomater. 75 (2018) 3–10, https://doi.org/10.1016/j.actbio.2018.05.019.
[108] A.C. Popa, G.E. Stan, M.A. Husanu, I. Pasuk, I.D. Popescu, A.C. Popescu, I. N. Mihailescu, Multi-layer haemocompatible diamond-like carbon coatings obtained by combined radio frequency plasma enhanced chemical vapor deposition and magnetron sputtering, J. Mater. Sci. Mater. Med. 24 (2013) 2695–2707, https://doi.org/10.1007/s10856-013-5026-y.
[109] S. Agathopoulos, D.U. Tulyaganov, J.M.G. Ventura, S. Kannan, M.A. Karakassides, J.M.F. Ferreira, Formation of hydroxyapatite onto glasses of the CaO–MgO–SiO2 system with B2O3, Na2O, CaF2 and P2O5 additives, Biomaterials. 27 (2006) 1832–1840, https://doi.org/10.1016/j.biomaterials.2005.10.033.
[110] D.U. Tulyaganov, S. Agathopoulos, P. Valerio, A. Balamurugan, A. Saranti, M. A. Karakassides, J.M.F. Ferreira, Synthesis, bioactivity and preliminary biocompatibility studies of glasses in the system CaO–MgO–SiO2–Na2O–P2O5–CaF2, J. Mater. Sci. Mater. Med. 22 (2011) 217–227, https://doi.org/10.1007/s10856-010-4203-5.
[111] T. Kokubo, H. Takadama, How useful is SBF in predicting in vivo bone bioactivity? Biomaterials. 27 (2006) 2907–2915, https://doi.org/10.1016/j.biomaterials.2006.01.017.
[112] International Organization for Standardization, ISO 23317:2014 Implants for surgery — In vitro evaluation for apatite-forming ability of implant materials,

Switz, Geneva, 2014 https://www.iso.org/obp/ui/#iso:std:iso:23317:ed-3:v1:en (accessed June 17, 2023.
[113] J.R. Jones, Review of bioactive glass: From Hench to hybrids, Acta Biomater. 9 (2013) 4457–4486, https://doi.org/10.1016/j.actbio.2012.08.023.
[114] A.C. Popa, H.R. Fernandes, M. Necsulescu, C. Luculescu, M. Cioangher, V. Dumitru, B.W. Stuart, D.M. Grant, J.M.F. Ferreira, G.E. Stan, Antibacterial efficiency of alkali-free bio-glasses incorporating ZnO and/or SrO as therapeutic agents, Ceram. Int. 45 (2019) 4368–4380, https://doi.org/10.1016/j.ceramint.2018.11.112.
[115] T. Tite, A.C. Popa, B.W. Stuart, H.R. Fernandes, I.M. Chirica, G.A. Lungu, D. Macovei, C. Bartha, L. Albulescu, C. Tanase, S. Nita, N. Rusu, D.M. Grant, J.M. F. Ferreira, G.E. Stan, Independent and complementary bio-functional effects of CuO and Ga2O3 incorporated as therapeutic agents in silica- and phosphate-based bioactive glasses, J. Mater. 8 (2022) 893–905, https://doi.org/10.1016/j.jmat.2021.12.009.
[116] A. Goel, S. Kapoor, R.R. Rajagopal, M.J. Pascual, H.-W. Kim, J.M.F. Ferreira, Alkali-free bioactive glasses for bone tissue engineering: A preliminary investigation, Acta Biomater. 8 (2012) 361–372, https://doi.org/10.1016/j.actbio.2011.08.026.
[117] P.P. Cortez, A.F. Brito, S. Kapoor, A.F. Correia, L.M. Atayde, P. Dias-Pereira, A. C. Maurício, A. Afonso, A. Goel, J.M.F. Ferreira, The in vivo performance of an alkali-free bioactive glass for bone grafting, FastOs®BG, assessed with an ovine model, J. Biomed. Mater. Res. Part B Appl. Biomater. 105 (2017) 30–38, https://doi.org/10.1002/jbm.b.33529.
[118] A.L.B. Maçon, T.B. Kim, E.M. Valliant, K. Goetschius, R.K. Brow, D.E. Day, A. Hoppe, A.R. Boccaccini, I.Y. Kim, C. Ohtsuki, T. Kokubo, A. Osaka, M. Vallet-Regí, D. Arcos, L. Fraile, A.J. Salinas, A.V. Teixeira, Y. Vueva, R.M. Almeida, M. Miola, C. Vitale-Brovarone, E. Verné, W. Höland, J.R. Jones, A unified in vitro evaluation for apatite-forming ability of bioactive glasses and their variants, J. Mater. Sci. Mater. Med. 26 (2015) 115, https://doi.org/10.1007/s10856-015-5403-9.
[119] J.G.C. Wolke, J.J.J.P. van den Beucken, J.A. Jansen, Growth behavior of rat bone marrow cells on RF magnetron sputtered bioglass- and calcium phosphate coatings, Key Eng. Mater. 361–363 (2008) 253–256, https://doi.org/10.4028/www.scientific.net/KEM.361-363.253.
[120] B.A.J.A. van Oirschot, R.M. Eman, P. Habibovic, S.C.G. Leeuwenburgh, Z. Tahmasebi, H. Weinans, J. Alblas, G.J. Meijer, J.A. Jansen, J.J.J.P. van den Beucken, Osteophilic properties of bone implant surface modifications in a cassette model on a decorticated goat spinal transverse process, Acta Biomater. 37 (2016) 195–205, https://doi.org/10.1016/j.actbio.2016.03.037.
[121] J.G.C. Wolke, K. van Dijk, H.G. Schaeken, K. de Groot, J.A. Jansen, Study of the surface characteristics of magnetron-sputter calcium phosphate coatings, J. Biomed. Mater. Res. 28 (1994) 1477–1484, https://doi.org/10.1002/jbm.820281213.
[122] J.E.G. Hulshoff, K. van Dijk, J.P.C.M. van Der Waerden, J.G.C. Wolke, L.A. Ginsel, J.A. Jansen, Biological evaluation of the effect of magnetron sputtered Ca/P coatings on osteoblast-like cellsin vitro, J. Biomed. Mater. Res. 29 (1995) 967–975, https://doi.org/10.1002/jbm.820290808.
[123] M. Ferraris, S. Perero, M. Miola, S. Ferraris, E. Verné, J. Morgiel, Silver nanocluster–silica composite coatings with antibacterial properties, Mater. Chem. Phys. 120 (2010) 123–126, https://doi.org/10.1016/j.matchemphys.2009.10.034.
[124] M. Ferraris, C. Balagna, S. Perero, M. Miola, S. Ferraris, F. Baino, A. Battiato, C. Manfredotti, E. Vittone, E. Vernè, Silver nanocluster/silica composite coatings obtained by sputtering for antibacterial applications, IOP Conf. Ser. Mater. Sci. Eng. 40 (2012), 012037, https://doi.org/10.1088/1757-899X/40/1/012037.
[125] F. Baino, S. Ferraris, M. Miola, S. Perero, E. Verné, A. Coggiola, D. Dolcino, M. Ferraris, Novel antibacterial ocular prostheses: Proof of concept and physico-chemical characterization, Mater. Sci. Eng. C. 60 (2016) 467–474, https://doi.org/10.1016/j.msec.2015.11.075.
[126] C. Balagna, S. Perero, E. Percivalle, E.V. Nepita, M. Ferraris, Virucidal effect against coronavirus SARS-CoV-2 of a silver nanocluster/silica composite sputtered coating, Open Ceram. 1 (2020), 100006, https://doi.org/10.1016/j.oceram.2020.100006.
[127] P.P. Poluektov, O.V. Schmidt, V.A. Kascheev, M.I. Ojovan, Modelling aqueous corrosion of nuclear waste phosphate glass, J. Nucl. Mater. 484 (2017) 357–366, https://doi.org/10.1016/j.jnucmat.2016.10.033.
[128] C.L. Thorpe, J.J. Neeway, C.I. Pearce, R.J. Hand, A.J. Fisher, S.A. Walling, N. C. Hyatt, A.A. Kruger, M. Schweiger, D.S. Kosson, C.L. Arendt, J. Marcial, C. L. Corkhill, Forty years of durability assessment of nuclear waste glass by standard methods, Npj Mater. Degrad. 5 (2021) 61, https://doi.org/10.1038/s41529-021-00210-4.
[129] I. Ahmed, H. Ren, J. Booth, Developing unique geometries of phosphate-based glasses and their prospective biomedical applications, Johnson Matthey, Technol. Rev. 63 (2019) 34–42, https://doi.org/10.1595/205651319X15426460058863.
[130] Q. Chen, J. Jing, H. Qi, I. Ahmed, H. Yang, X. Liu, T.L. Lu, A.R. Boccaccini, Electric field-assisted orientation of short phosphate glass fibers on stainless steel for biomedical applications, ACS Appl. Mater. Interfaces. 10 (2018) 11529–11538, https://doi.org/10.1021/acsami.8b01378.
[131] G. Novajra, N.G. Boetti, J. Lousteau, S. Fiorilli, D. Milanese, C. Vitale-Brovarone, Phosphate glass fibre scaffolds: Tailoring of the properties and enhancement of the bioactivity through mesoporous glass particles, Mater. Sci. Eng. C. 67 (2016) 570–580, https://doi.org/10.1016/j.msec.2016.05.048.
[132] C. Tan, I. Ahmed, A.J. Parsons, C. Zhu, F.B. Betanzos, C.D. Rudd, X. Liu, Effects of Fe2O3 addition and annealing on the mechanical and dissolution properties of MgO-and CaO-containing phosphate glass fibres for bio-applications, Biomed. Glas. 4 (2018) 57–71, https://doi.org/10.1515/bglass-2018-0006.
[133] K.M.Z. Hossain, U. Patel, A.R. Kennedy, L. Macri-Pellizzeri, V. Sottile, D.M. Grant, B.E. Scammell, I. Ahmed, Porous calcium phosphate glass microspheres for orthobiologic applications, Acta Biomater. 72 (2018) 396–406, https://doi.org/10.1016/j.actbio.2018.03.040.
[134] I. Ahmed, I.A. Jones, A.J. Parsons, J. Bernard, J. Farmer, C.A. Scotchford, G. S. Walker, C.D. Rudd, Composites for bone repair: phosphate glass fibre reinforced PLA with varying fibre architecture, J. Mater. Sci. Mater. Med. 22 (2011) 1825–1834, https://doi.org/10.1007/s10856-011-4361-0.
[135] F. Alshomer, C. Chaves, T. Serra, I. Ahmed, D.M. Kalaskar, Micropatterning of nanocomposite polymer scaffolds using sacrificial phosphate glass fibers for tendon tissue engineering applications, Nanomedicine Nanotechnology, Biol. Med. 13 (2017) 1267–1277, https://doi.org/10.1016/j.nano.2017.01.006.
[136] B.W. Stuart, J.W. Murray, D.M. Grant, Two step porosification of biomimetic thin-film hydroxyapatite/alpha-tri calcium phosphate coatings by pulsed electron beam irradiation, Sci. Rep. 8 (2018) 14530, https://doi.org/10.1038/s41598-018-32612-x.
[137] F. Huang, C. Ye, H. He, Y. Liu, X. Wang, Z. Ning, Effect of driving frequency on plasma property in radio frequency and very high frequency magnetron sputtering discharges, Plasma Sources Sci. Technol. 23 (2013), 015003, https://doi.org/10.1088/0963-0252/23/1/015003.
[138] P. Yang, C. Ye, X. Wang, J. Guo, S. Zhang, Control of growth and structure of Ag films by the driving frequency of magnetron sputtering, Plasma Sci. Technol. 19 (2017), 085504, https://doi.org/10.1088/2058-6272/aa6619.
[139] A. Shearer, M. Montazerian, J.C. Mauro, Modern definition of bioactive glasses and glass-ceramics, J. Non. Cryst. Solids. 608 (2023), 122228, https://doi.org/10.1016/j.jnoncrysol.2023.122228.
[140] K. Ishii, H. Nakayama, Structural relaxation of vapor-deposited molecular glasses and supercooled liquids, Phys. Chem. Chem. Phys. 16 (2014) 12073–12092, https://doi.org/10.1039/C4CP00458B.
[141] A. Gujral, K.A. O'Hara, M.F. Toney, M.L. Chabinyc, M.D. Ediger, Structural characterization of vapor-deposited glasses of an organic hole transport material with X-ray scattering, Chem. Mater. 27 (2015) 3341–3348, https://doi.org/10.1021/acs.chemmater.5b00583.
[142] K.J. Dawson, L. Zhu, L. Yu, M.D. Ediger, Anisotropic structure and transformation kinetics of vapor-deposited indomethacin glasses, J. Phys. Chem. B. 115 (2011) 455–463, https://doi.org/10.1021/jp1092916.
[143] W.-Y. Liu, Z.-W. Fu, C.-L. Li, Q.-Z. Qin, Lithium phosphorus oxynitride thin film fabricated by a nitrogen plasma-assisted deposition of e-beam reaction evaporation, Electrochem. Solid-State Lett. 7 (2004) J36, https://doi.org/10.1149/1.1778934.
[144] S.M. Baumann, C.C. Martner, D.W. Martin, R.J. Blattner, A.J. Braundmeier, A study of electron beam evaporated SiO2, TiO2, and Al2O2 films using RBS, HFS, and SIMS, Nucl. Instruments Methods Phys. Res. Sect. B Beam Interact. with Mater. Atoms. 45 (1990) 664–668, https://doi.org/10.1016/0168-583X(90)90921-G.
[145] A.D. Yeadon, S.J. Wakeham, H.L. Brown, M.J. Thwaites, M.J. Whiting, M. A. Baker, Remote plasma sputtering of indium tin oxide thin films for large area flexible electronics, Thin Solid Films. 520 (2011) 1207–1211, https://doi.org/10.1016/j.tsf.2011.07.072.